Tornado Vortex Structure, Intensity, and Surface Wind Gusts in Large-Eddy Simulations with Fully Developed Turbulence

DAVID S. NOLAN AND NATHAN A. DAHL

Rosenstiel School of Marine and Atmospheric Science, University of Miami, Miami, Florida

GEORGE H. BRYAN AND RICHARD ROTUNNO

National Center for Atmospheric Research,[a] *Boulder, Colorado*

(Manuscript received 2 September 2016, in final form 17 March 2017)

ABSTRACT

A large-eddy simulation (LES) framework with an ''eddy injection'' technique has been developed that ensures a majority of turbulent kinetic energy in numerically simulated tornado-like vortices is represented by resolved eddies. This framework is used to explore the relationships between environmental forcing mechanisms, surface boundary conditions, and tornado vortex structure, intensity, and wind gusts. Similar to previous LES studies, results show that the maximum time- and azimuthal-mean tangential winds $\{V\}_{\max}$ can be well in excess of the ''thermodynamic speed limit,'' which is 66 m s^{-1} for most of the simulations. Specifically, $\{V\}_{\max}$ exceeds this speed by values ranging from 21% for a large, high-swirl vortex to 59% for a small, low-swirl vortex. Budgets of mean and eddy angular and radial momentum are used to show that resolved eddies in the tornado core act to reduce the wind speed at the location of $\{V\}_{\max}$, although they do transport angular momentum downward into the lowest levels of the boundary layer, increasing low-level swirl.

Three measures of tornado intensity are introduced: maximum time–azimuthal-mean surface (10 m) horizontal wind speed ($\{S10\}_{\max}$), maximum 3-s gusts of S10 (S10-3s), and maximum vertical 3-s gusts at 10 m (W10-3s). While $\{S10\}_{\max}$ is considerably less than $\{V\}_{\max}$, transient features in the boundary layer can generate S10-3s in excess of 150 m s^{-1}, and W10-3s in excess of 100 m s^{-1}. For high-swirl vortices, the extreme gusts are confined closer to the center, well inside the radius of maximum azimuthal-mean surface winds. For the low-swirl vortex, both the strongest mean winds and the extreme gusts are restricted to a very narrow core.

1. Introduction

a. Motivation

The advent in the 1990s of portable Doppler radars (e.g., Bluestein et al. 1993; Wurman et al. 1996) led to significant advances in the observation of wind fields in and around tornadoes. Here we are referring to tornadoes associated with supercell thunderstorms that often cause significant damage and, occasionally, loss of life. Because of the remarkable efforts of many scientists and the continuing support of U.S. government agencies, over the last 20 years the tornado research community has obtained a large number of Doppler radar analyses of tornadoes (e.g., Rasmussen et al. 1994; Wurman 1998, 2008; Wurman et al. 2012). For example, the brief survey by Alexander and Wurman (2008) documents over 5000 individual Doppler radar swaths through 69 different tornadoes over a period of 9 years, and this is only a subset of such observations. Although tornadoes can exhibit a wide variety of structures and behaviors (Bluestein and Golden 1993; Davies-Jones et al. 2001), a fairly consistent picture has emerged from these numerous cases. Maximum ground-relative wind speeds for such tornadoes typically range from 50 to 100 m s^{-1}, with some observations indicating wind speeds in excess of 120 m s^{-1} (Bluestein et al. 1993; Wurman et al. 2013; Snyder and Bluestein 2014). The fastest horizontal wind speeds usually occur fairly close to the surface, near the top of an inflow layer that generally appears to be tens of

[a] The National Center for Atmospheric Research is sponsored by the National Science Foundation.

Corresponding author e-mail: David S. Nolan, dnolan@rsmas.miami.edu

DOI: 10.1175/JAS-D-16-0258.1

meters deep but could be as shallow as 5 m (Kosiba and Wurman 2013).

Of course, the part of the tornado wind field that is of most interest to the public is the part very close to the surface, 30 m or less above ground level (AGL). Unfortunately, radar observations of the wind field below 30 m are quite rare. This is for many reasons, including spreading of the radar beam, interference from natural and manmade structures, and changes in elevation of the land surface between the tornado and the radar. In a few ''serendipitous'' cases, portable Doppler radars have come within a few hundred meters of tornadoes, allowing for some uncontaminated radar swaths to pass through the wind field at or below 10 m AGL (Wurman et al. 2007; Kosiba and Wurman 2013; Weiss et al. 2014). These observations are less reliable because they are more likely to contain debris, which, because of centrifugal forces, does not move precisely with the local wind (Dowell et al. 2005).

In situ wind observations near the surface and in the cores of significant tornadoes are quite rare, but they have occurred. For example, a mobile mesonet vehicle caught in a tornado in 2007 reported a 1-s gust of 50 m s^{-1} at about 2.9 m AGL (Blair et al. 2008). A fixed instrument in an Arizona forest (although located in a relatively wide-open area) survived a direct hit from a tornado, reporting a 1-s gust of 72 m s^{-1} at 2.5 m AGL (Blanchard 2013). Another mobile mesonet vehicle, working in tandem with one of the Doppler on Wheels radars (DOWs), was caught in a newly formed tornado and reported 43 m s^{-1} at 3.5 m AGL (Kosiba and Wurman 2013; averaging interval was not stated). A few observations have been acquired intentionally, such as by the Tornado Intercept Vehicle (TIV), reporting 1-s wind speeds of 58 m s^{-1} at 3.5 m AGL in a tornado in 2009 (Wurman et al. 2013).

In the latter two cases, the simultaneous proximity of a DOW allowed for the rare direct comparison of near-surface to above-surface wind speeds. These are informative, but for the purposes of constructing a three-dimensional view of the near-surface wind field, they are very limited: the in situ measurements represent a single point and exhibit high-frequency variability. The radar observations are representative of the reflectivity-weighted wind in a volume of air and are not continuous in time (Snyder and Bluestein 2014). The decomposition of either into tornado-relative tangential (V) and radial (U) winds relies on accurate knowledge of the location and motion of the circulation center and an assumption of vortex symmetry.

In contrast to point measurements and vertical profiles, some studies have attempted to reconstruct the axisymmetric-mean tornado wind field through the more comprehensive analysis of Doppler wind observations known as ground-based velocity track display (GBVTD; Lee et al. 1999; Bluestein et al. 2003; Lee and Wurman 2005). While this method appears to work well for V at and above the lowest observing level, recent studies have identified large sensitivities of the analyzed U and vertical wind W to unknown quantities such as the outward motion of centrifuged debris (Dowell et al. 2005; Wakimoto et al. 2012) and the radial inflow between the lowest observing level and the surface (Nolan 2013). Therefore, despite the enormous amount of invaluable data that has been accumulated from numerous Doppler radar samples, the typical structures and intensities of the wind field in the tornado boundary layer remain uncertain.

In stark contrast, numerical simulations of tornadoes provide a complete and continuous view of the near-surface flow in a tornado. Despite the known difficulties for any fluid dynamical model to resolve or represent turbulence (e.g., Sullivan et al. 1994; Brasseur and Wei 2010), numerical simulations do perform extremely well in terms of conservation of mass and conservation of momentum (energy may be less well conserved). Tornadic flow structures predicted by models, while perhaps erroneous in some details, will at least be consistent with these constraints.

Further, simulations have the potential to provide useful insight into aspects of the tornado wind field that, to our knowledge, have not been systematically considered. These include the relationships between localized wind gusts (at the surface, or aloft), azimuthal-mean winds (the ''symmetric'' circulation), and time-mean winds. Note that here ''time mean'' indicates an average over a specified period, such as a few minutes for a large, quasi-steady-state tornado. For example, suppose a Doppler radar measures a peak difference of wind speeds toward and away from the radar—often called ΔV—of 100 m s^{-1} separated by a distance of 200 m. This suggests an instantaneous maximum tangential wind $[V]_{\max} = 50$ m s^{-1} (where herein the square brackets denote an azimuthal mean around a vortex center) at a radius of maximum tangential wind RMV = 100 m. But this observation is only representative of the winds of two radar volumes along a line perpendicular to the observer and is not the same as the instantaneous, azimuthal-mean wind $[V]_{\max}$. Is $[V]_{\max}$, on average, approximately the same value? Or is it systematically less because we are selecting a maximum observed ΔV? Indeed, analyses that infer the azimuthal-mean wind from collected Doppler radar observations, such as those using the GBVTD technique, consistently produce values for $[V]_{\max}$ that are less than half the contemporaneous values of ΔV

(Bluestein et al. 2003; Tanamachi et al. 2007; Kosiba et al. 2008; Kosiba and Wurman 2010).

Moving in the other direction, for a given value of $[V]_{max}$, what are the expected values of the maximum mean tangential flow at the surface $[V10]_{max}$, the maximum azimuthal-mean surface radial inflow $[U10]_{max}$, and maximum azimuthal-mean surface wind speed $[S10]_{max}$? Most importantly of all, what are the expected mean values and variabilities of short-term wind speeds, such as 3-s gusts at 10-m height, which are used to predict damage and, in turn, are diagnosed from damage surveys? For the foreseeable future, such questions can only be addressed by numerical simulations.

b. An improved tornado modeling framework

Of course, the answers these simulations provide will only be as accurate as are the simulations themselves in reproducing the dynamics of the tornado boundary layer. With the astonishing increases in computer power over the last 20 years, tornado simulations appear to have become increasingly realistic (e.g., Fiedler 1998, 2009; Lewellen et al. 1997, 2000; Lewellen and Lewellen 2007a,b; Lewellen et al. 2008; Kuai et al. 2008). In this discussion, we are referring to simulations designed to represent only the tornado vortex itself, with the effects of the parent thunderstorm—upward motion and rotation—provided through boundary conditions or other modeling techniques. In a companion paper (Bryan et al. 2017, hereafter B17) we argue that some previous large-eddy simulations (LESs) have been unsatisfactory in one important manner: in the boundary layer flow swirling into the tornado core, the effects of turbulence have been almost entirely represented by a subgrid-scale (SGS) mixing scheme, rather than by resolved turbulent eddies. This is not entirely due to insufficiently small grid spacings. Since the far-field environment in most such simulations is relatively quiescent, and usually even less well resolved because of grid-stretching techniques, the air that flows into the tornado boundary layer may not contain resolved turbulent eddies. While the vertically varying diffusion profiles of an SGS scheme can allow wind profiles near the surface to be much sharper (with faster winds near the surface) than a lower–Reynolds number simulation would allow, this cannot give us confidence that the effects of turbulence are being represented correctly.

B17 introduces a method to ''inject'' turbulence into the boundary layer. The method involves using a precursor, 3D, LES of boundary layer flow in a relatively small rectangular domain that is driven by a specified wind speed at the top of a boundary layer produced from another, precursor, axisymmetric tornado simulation. Velocity perturbations in the 3D precursor simulation are saved every few time steps. These perturbations are then added, through a nudging technique, to the boundary layer inflow in a ring of radius 2 km around the center of our simulated tornado. The results of B17 show that producing these resolved eddies in the boundary layer leads to notable changes in the inner-core structure and intensity of simulated tornadoes.

c. Goals of this study

Using the improved methodology of B17, this paper will explore the inner-core dynamics of tornadoes and how these dynamics change as the vortex size, intensity, and surface properties underneath the vortex are varied. In addition, for each case we will compute a hierarchy of measures of tornado intensity, such as the time–azimuthal-mean wind aloft, the time–azimuthal-mean wind at the surface, and maximum 3-s-average winds at the surface. These are herein referred to as 3-s gusts, with the 3-s time period chosen to match how winds are described in the enhanced Fujita tornado damage scale (WSEC 2006). In subsequent papers, we will extend this work to more realistically simulated observations, both from in situ sensors in the path of the tornado and from radars.

2. Modeling framework and parameters

Our tornado modeling framework takes the ''Fiedler chamber'' approach (Fiedler 1994; Nolan 2005; Rotunno 2013) of using a large closed domain, a fixed vertical forcing function, and a constant background rotation. A discussion of this framework is given in Rotunno et al. (2016, hereafter R16). An additional feature is the use of a Rayleigh damping function on the velocity fields in the upper part of the domain, with the specific (and important) purpose of suppressing the recirculation of turbulent eddies that are generated in the outflow of the simulated tornado. Without this damping, some of these eddies will recirculate back to the surface and unrealistically influence the structure and intensity of the vortex.

The underlying numerical model is CM1 (Bryan and Fritsch 2002). The equations of motion are stated in R16 and in B17; they describe the evolution of an isentropic, nearly incompressible fluid with a sound speed that is fixed to be constant everywhere at $c = 300\,\mathrm{m\,s^{-1}}$. B17 provides full details of the ''eddy injection'' method to introduce turbulence into the boundary layer. Also described in B17 is the initialization procedure, in which an axisymmetric model is first integrated to an approximate steady state, and this flow field is then interpolated to a three-dimensional grid.

For convenience we repeat here some of the basic parameters of the framework. The model uses equations of motion for a constant-density, nearly incompressible fluid with a fixed sound speed $c_s = 300\,\mathrm{m\,s^{-1}}$ [see (1a)–(1d) of R16]. In an earlier study, Xia et al. (2003) found that differences in vortex structure and intensity were relatively small when comparing simulations with incompressible and fully compressible equation sets. All simulations are performed in a square domain, 40 km on each side and 15 km deep. For the control configurations used for most of the results below, the number of grid cells in the x, y, and z directions are $1120 \times 1120 \times 512$. The grid-stretching capability of CM1 is used to pack grid points densely near the center, such that the horizontal grid spacings are 5 m inside a 4 km × 4 km box at the center of the domain, and the vertical spacings are 2.5 m between the surface and $z = 1$ km. Outside this high-resolution volume the grid spacings expand to 220 m in the horizontal and 248 m in the vertical. Additional simulations are presented using $\Delta x = 20$, 10, and 2.5 m, with $\Delta z = \Delta x/2$ in each case.

All simulations use the same vertical forcing function as in R16 and B17 [see (3) and (4) of R16], centered at $x = 0$, $y = 0$, and $z_b = 8$ km, with half-depth $l_z = 7$ km and half-width $l_r = 3$ km. The upper-damping zone is also identical, varying like a cosine function from zero to maximum amplitude between $z_d = 8$ km and the domain top at $z = 15$ km [(4) of R16]. The strength of the vertical forcing is chosen so that an unimpeded parcel rising up along its center axis would achieve a vertical speed of $80\,\mathrm{m\,s^{-1}}$; this speed defines the convective velocity scale W_{conv}. However, in our simulations this velocity is diminished because of the large overlap of the damping layer and the forcing (Fig. 2 of R16) and the effect of the model ceiling at $z = 15$ km. The effective velocity scale, computed from a three-dimensional, LES simulation without rotation or eddy injection, is $W_{\mathrm{eff}} = 65.8\,\mathrm{m\,s^{-1}}$.

3. Results

a. Control case

As discussed in R16, a nondimensional parameter that describes the influence of rotation in these simulations is a swirl ratio based on the radial scale of the convective forcing, $S_r = \Omega l_r / W_{\mathrm{conv}}$. For the control case (CTRL), we use $S_r = 0.01$, meaning that $\Omega = 2.667 \times 10^{-4}\,\mathrm{s^{-1}}$. This value was chosen because it produces a vortex with a radius of maximum tangential velocity, RMV, equal to 152 m. This is close to the median value diagnosed from the survey of radar observations by Alexander and Wurman (2008). CTRL uses a surface roughness $z_0 = 0.2$ m (equivalent to cropland with scattered obstacles).

TABLE 1. Names and parameters for the simulations used in this study. An asterisk indicates the same value as for the control simulation (CTRL).

Name	$\Delta x/\Delta z$ (m)	W_{conv} ($\mathrm{m\,s^{-1}}$)	S_r	z_0 (m)
CTRL	5/2.5	80	0.01	0.2
CTRL20	20/10	*	*	*
CTRL10	10/5	*	*	*
CTRL2.5	2.5/1.25	*	*	*
SR02	*	*	0.02	*
SR005	*	*	0.005	*
Z0-8	*	*	*	0.8
Z0-05	*	*	*	0.05
W40	*	40	*	*
W60	*	60	*	*
W100	*	100	*	*

The input parameters and names of all the simulations are summarized in Table 1.

After the 3D simulations have reached steady state, samples of the 3D fields are taken every 1 s for 300 s. These fields are used for computing time–azimuthal means, eddy fluxes, and other statistics. For the results in this section, azimuthal-mean fields are computed relative to a vortex center defined by the centroid of the negative pressure anomaly averaged over the lowest 50 m. Figure 1a shows contours of $\{V\}$ and vectors of $\{U\}$ and $\{W\}$: we use $\{\cdot\}$ to indicate the time- and azimuthal-mean fields.

The basic characteristics of the mean vortex shown in Fig. 1a are quite similar to those shown in many previous studies using both axisymmetric and three-dimensional models (e.g., Rotunno 1979; Howells et al. 1988; Fiedler 1994, 1998; Nolan and Farrell 1999; Nolan 2005; Lewellen et al. 1997, 2000). The mean tangential wind $\{V\}$ is maximized in the upper portion of the inflow layer, while the inflow $\{U\}$ is maximized closer to the surface. In the boundary layer, both $\{U\}$ and $\{V\}$ increase toward the center until they reach their maximum values around $r = 200$ and 150 m, respectively. Inside the RMV, the flow turns upward and then rebounds outward with nearly the same speed at which it entered the corner region. Radial inflow is weak (about $5\,\mathrm{m\,s^{-1}}$; see Fig. 1c) at the location of $\{V\}_{\max}$; it cannot be zero there (Kepert 2001; Nolan 2013).

The value for $\{V\}_{\max}$ for this simulation is $93\,\mathrm{m\,s^{-1}}$. This clearly exceeds W_{eff} ($66\,\mathrm{m\,s^{-1}}$) and even W_{conv} ($80\,\mathrm{m\,s^{-1}}$). A time–azimuthal-mean wind well in excess of W_{eff} stands in contrast to the findings of many earlier studies, both axisymmetric and three-dimensional, that used constant eddy viscosity and no-slip boundary conditions (Fiedler 1994, 1998, 2009; Nolan 2005). However, when using much higher Reynolds numbers than those earlier studies, the axisymmetric simulations of R16 produced $\{V\}_{\max}$ values that also exceed W_{eff} by over 70%.

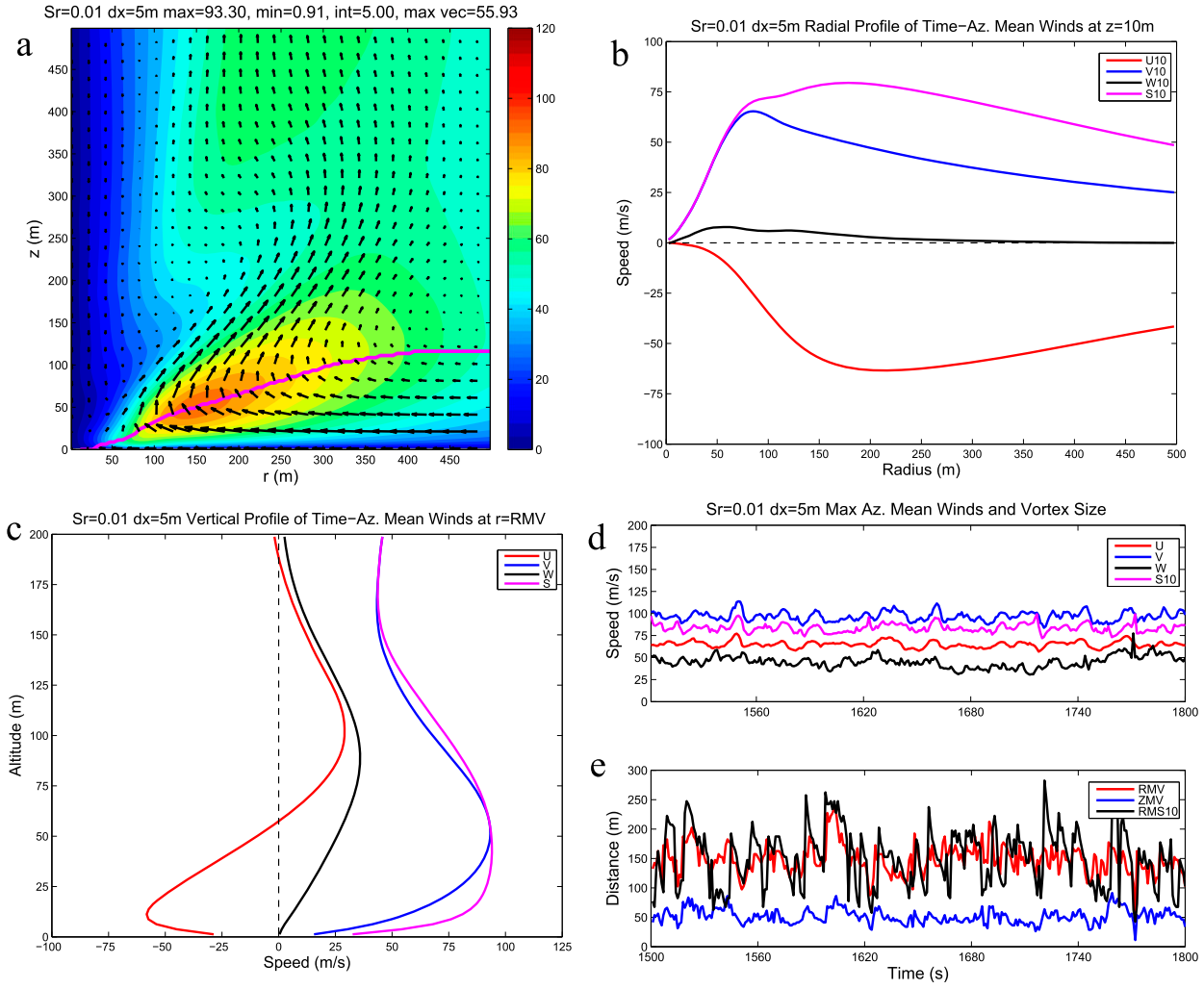

FIG. 1. Time–azimuthal-mean and azimuthal-mean wind fields for the simulation CTRL: (a) time–azimuthal-mean tangential winds (colors) and secondary circulation (vectors), along with the depth of the inflow layer (magenta line), defined as the height where $-U$ is equal to 10% of the fastest inflow anywhere in the boundary layer $\{-U\}_{\max}$; (b) radial profiles of time–azimuthal-mean U, V, W, and horizontal wind S at $z = 10$ m; (c) vertical profiles of U, V, W, and S at $r =$ RMV; (d) time series of maximum azimuthal-mean U, V, W, and S10; (e) time series of the radius and height where $\{V\}_{\max}$ occurs, and the radius where $\{\text{S10}\}_{\max}$ occurs. In (a) and subsequent figures, the vectors are plotted every 20 m.

The magenta curve in Fig. 1a shows the depth of the inflow layer, following the definition proposed by Zhang et al. (2011) for hurricanes, which is the height where $\{-U\}_{\max}$ first decreases to 10% of its maximum value in the boundary layer. For CTRL, the fastest inflow speed is 63.6 m s^{-1}; therefore the inflow layer is defined by $U < -6.4$ m s^{-1}. While using $U = 0$ would be a natural choice, it can produce highly variable results as the vertical gradient of U also becomes very small near the top of the layer. Note also that the location of $\{V\}_{\max}$ occurs very close to the magenta curve—that is, very close to the top of the inflow layer by this definition.

Further details of the boundary layer can be seen more clearly in radial and vertical profiles as shown in Figs. 1b and 1c. For $r > 125$ m, $\{U\}$ at 10 m is actually greater than $\{V\}$, which is consistent with recent damage surveys of strong tornadoes in urban and wooded environments (Karstens et al. 2013, Atkins et al. 2014; Burgess et al. 2014). This can also be seen in the vertical profiles. While $\{V\}_{\max} = 93.3$ m s^{-1}, the peak mean horizontal wind at the surface $\{\text{S10}\}_{\max}$ is only 79.5 m s^{-1}. Interestingly, where S10 is largest, most of its contribution comes from U10, and as a result, the radius at which the fastest mean surface winds occur (RMS10) is 177.5 m, outside the RMV. Furthermore, values of S10 exceeding 50 m s^{-1} extend out to almost 500 m from the center of the vortex. This is also consistent with damage surveys for significant tornadoes, which often show moderate

TABLE 2. Time–azimuthal-mean vortex sizes and intensities. Mean sizes and intensities for the simulated tornado vortices in this study, including radius of maximum tangential wind (RMV), height of maximum tangential wind (ZMV), and radius of maximum S10 (RMS10), where S10 refers to horizontal wind speed at 10-m height.

Name	$\{V\}_{max}$ (m s^{-1})	RMV (m)	ZMV (m)	$\{-U\}_{max}$ (m s^{-1})	$\{W\}_{max}$ (m s^{-1})	$\{S10\}_{max}$ (m s^{-1})	RMS10 (m)
CTRL	93.3	152.5	51.3	63.6	38.4	79.5	177.5
CTRL20	94.3	150.0	45.0	61.1	35.3	77.2	170.0
CTRL10	93.6	135.0	42.5	64.6	34.0	78.6	155.5
CTRL2.5	97.8	143.8	49.4	65.9	42.1	86.5	163.8
SR02	80.0	282.5	56.3	52.1	21.4	67.8	322.5
SR005	104.9	47.5	31.3	70.0	92.1	97.7	27.5
Z0-8	92.1	147.5	71.3	63.7	48.7	70.3	72.5
Z0-05	99.1	137.5	31.3	67.0	34.5	92.9	142.5
W40	49.1	92.5	36.3	34.0	21.7	43.6	107.5
W60	72.0	117.5	43.8	48.3	32.3	61.3	142.5
W100	121.3	162.5	56.3	83.6	51.1	101.3	197.5

wind damage extending hundreds of meters from the analyzed center.

Figure 1d shows time series of the time-evolving maxima of the azimuthal-mean fields and their locations. The azimuthal-mean vortex structure shows only minor deviations in size or intensity. There are quasi-periodic oscillations in both, with periods appearing to range from 5 to 20 s. The location of $[S10]_{max}$ shows large variations, but this is because of the fairly flat profile of S10 (Fig. 1c), such that a relatively small, localized increase will relocate the maximum value.

The structural properties of the time-azimuthal-mean vortex are listed in Table 2. In Table 3, four additional measures of intensity are shown: the maximum and mean values of the peak surface 3-s wind gust (S10-3s) occurring anywhere, such as what might be occurring in suction vortices, wind streaks, or other transient structures in the tornado, and also the maximum and mean values of the peak vertical wind gusts (W10-3s). To compute 3-s gusts, wind data at the 10-m level were saved every 0.1 s and the 3-s gusts are running averages over the previous 30 outputs at fixed points. To illustrate the difference, Fig. 2 shows horizontal slices of instantaneous values and 3-s gusts of S10 at the same time. The peak values of S10-3s are considerably reduced, and they show swathlike features that lag behind the instantaneous maxima, showing the paths that those localized wind maxima have taken over the previous 3 s; these paths are marked by the black lines in Fig. 2b. Also shown in Fig. 2 are time series of the peak instantaneous S10, S10-3s, and the mean value of S10-3s. The 3-s gusts are considerably less than instantaneous wind speeds, and this demonstrates the importance of using some relevant averaging period. The instantaneous values, while amazingly large, only exist in each place and time for about a tenth of a second, as will be shown later. While the peak 3-s gust at any time is also interesting, Fig. 2c shows that the most extreme values occur randomly and only a few times in the 5-min period. Therefore, the time mean of maximum S10-3s (solid black line) is a more representative indicator of the intensity of, and the general damage that would be caused by, a fully turbulent tornado. This measure of intensity is analogous to the ''best track'' intensity used to describe

TABLE 3. Time-mean maximum and peak maximum values of 3-s gusts of horizontal and vertical winds at $z = 10$ m, S10-3s, and W10-3s. The time–azimuthal-mean tangential wind is included for reference.

Name	$\{V\}_{max}$ (m s^{-1})	Mean max S10-3s (m s^{-1})	Max S10-3s (m s^{-1})	Mean max W10-3s (m s^{-1})	Max W10-3s (m s^{-1})
CTRL	93.3	108.5	130.5	28.4	74.3
CTRL20	94.3	83.5	89.6	15.2	18.5
CTRL10	93.6	97.7	116.2	24.7	65.2
CTRL2.5	97.8	109.9	133.0	28.9	59.3
SR02	80.0	98.1	121.8	21.0	32.8
SR005	104.9	131.1	180.9	118.2	190.9
Z0-8	92.1	107.1	144.1	32.2	72.1
Z0-05	99.1	113.9	133.8	24.9	35.0
W40	49.1	60.0	76.0	25.4	52.6
W60	72.0	86.9	105.1	25.9	70.8
W100	121.3	133.3	156.5	32.1	69.7

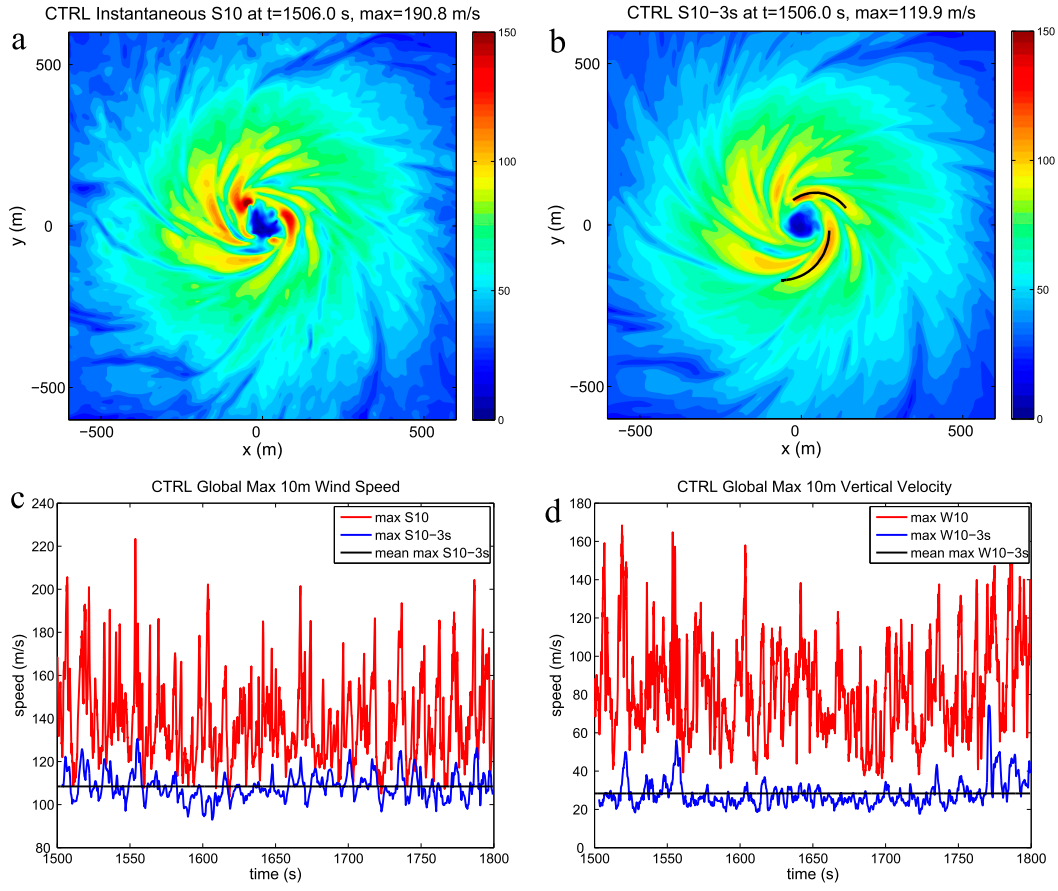

FIG. 2. Instantaneous and 3-s gusts of horizontal and vertical winds at $z = 10$ m for CTRL: (a) selected snapshot of instantaneous S10; (b) S10-3s at the same time; (c) time series of maximum instantaneous and 3-s gusts of S10; (d) time series of maximum instantaneous and 3-s gusts of W10. The black lines in (b) indicate the paths of smaller-scale vortices that trace out "swaths" in the 3-s-averaged wind field.

hurricanes, which is a 6-h representative value of the peak 1-min wind that is associated with the storm (Landsea and Franklin 2013; Nolan et al. 2014).

Finally, also shown in Fig. 2d are time series of instantaneous and 3-s gusts of W at 10-m height (W10-3s). The peak instantaneous values of W10 are astonishingly large, ranging from 40 to 160 m s^{-1}, but as noted above they are extremely brief. As shown in Table 3, a true 3-s upward gust of 74.3 m s^{-1} does occur, but it can be seen from Fig. 2d that a 10-m updraft this strong occurs only once during the 5-min simulation. Thus maximum peak values of W10-3s are even less representative of intensity and damage potential than the maximum values of S10-3s. Nonetheless, the remarkably strong updrafts that occur in this and subsequent vortices help us to understand how large debris can be lifted from the surface in strong tornadoes.

In preliminary simulations for R16, the domain size, domain height, the shape of the vertical forcing function, and the depth of the damping layer were extensively varied to find configurations for which the final outcomes—vortex structure and intensity—were not significantly dependent on such parameters. Nonetheless, some of the numerical results in Table 2 may be sensitive to some of the model parameters that are not varied in this study. As noted below in section 3f, we did find some dependence of the RMV on the damping-layer relaxation rate.

b. *Resolution sensitivity*

For any modeling study it is important to consider to what extent the results depend on the resolution. For comparison, we present simulations like CTRL but with $\Delta x = 20$, 10, and 2.5 m (CTRL20, CTRL10, and CTRL2.5, respectively), again with $\Delta z = \Delta x/2$ in each case. The computational cost and data storage challenges of the 2.5-m simulation prohibited us from using it as the standard resolution, although we did perform a single simulation for validation. These simulations were performed in exactly the same way, including the

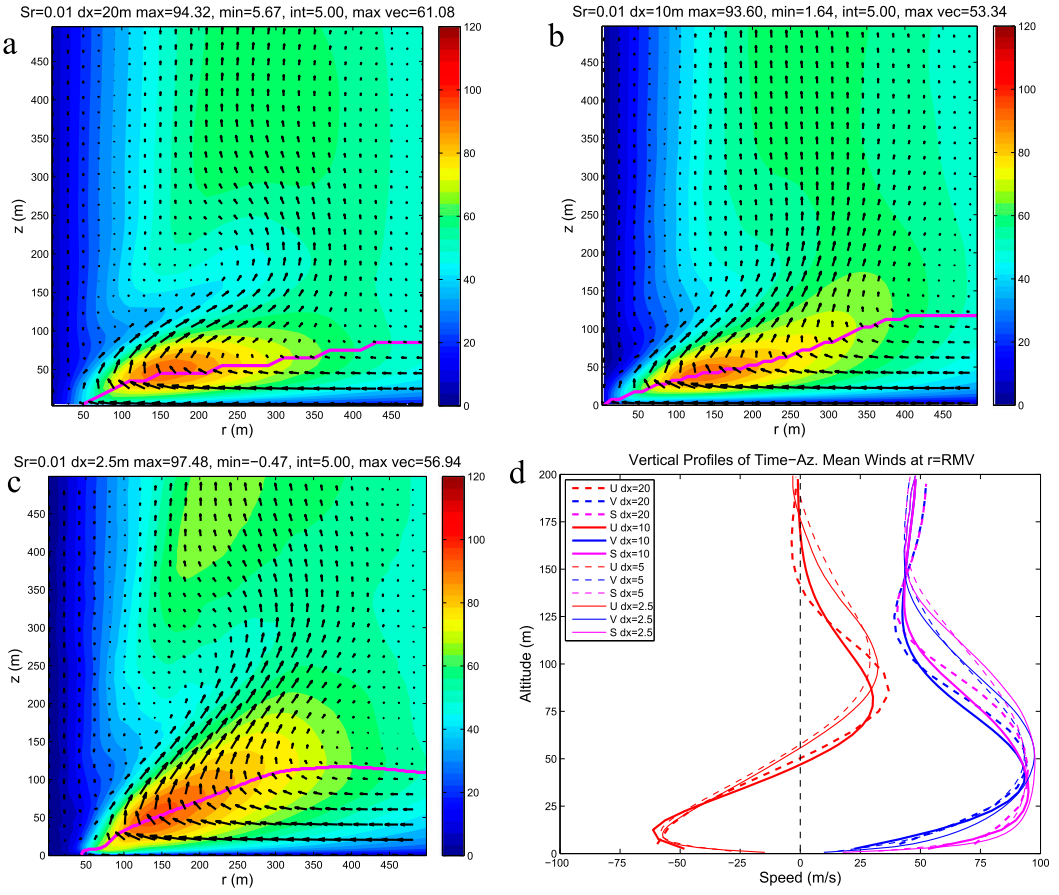

FIG. 3. Time–azimuthal-mean wind fields for simulations with varying resolution: (a) CTRL20 ($\Delta x = 20$ m, $\Delta z = 10$ m); (b) CTRL10; (c) CTRL2.5; (d) vertical profiles of wind speeds at each of their respective RMVs. As in Fig. 1, the magenta curves in (a)–(c) show the depth of the inflow layer as defined by 10% of $\{-U\}_{\max}$.

axisymmetric precursor simulation and the eddy-injection technique, with the resolution for each adjusted to match the final simulation.

Figure 3 shows the results for different resolutions. The $\Delta x = 20$ m case (CTRL20) has a shallower boundary layer, its RMV is slightly smaller, and its $\{V\}_{\max}$ is slightly greater than for $\Delta x = 5$ (Fig. 1a). For CTRL10, the boundary layer depth and the vortex size are also slightly smaller than for CTRL. For CTRL2.5, the time- and azimuthal-mean structure and intensity are slightly larger than for CTRL, but smaller than for CTRL10, while its $\{V\}_{\max}$ is notably larger: 97.8 m s^{-1}. Vertical profiles of $\{U\}$ and $\{V\}$ at the RMV, as shown in Fig. 3d, show little qualitative differences between the four cases.

These results are also listed in Tables 2 and 3. We see that the time-mean peak wind gusts (S10-3s) increase significantly from CTRL20 (83.5 m s^{-1}) to CTRL10 (97.7 m s^{-1}) to CTRL (108.5 m s^{-1}). The fact that it only increases to 109.5 m s^{-1} for CTRL2.5 suggests that the representation of small-scale structures in the tornado is beginning to converge for these grid spacings. Similarly, the mean peak W10-3s increases only from 28.4 to 28.9 m s^{-1}.

These decreasing differences are illustrated by time series of peak S10 and peak S10-3s computed from wind fields that are spatially averaged and compared to output from simulations with equivalent resolutions. Figure 4 shows time series from CTRL and CTRL10, where the 10-m winds from CTRL were first horizontally averaged to match the resolution of CTRL10. The instantaneous peaks of S10 from spatially averaged CTRL are about 40 m s^{-1} greater than those of CTRL10, while the time-mean S10-3s is about 10% greater. In CTRL2.5 versus CTRL, the spatially averaged instantaneous winds are only about 20 m s^{-1} greater than those of CTRL, while the peak and mean peak values for S10-3s are nearly identical. The dynamical structures that produce these extreme winds are further discussed in section 3d.

Some convergence of the results is also suggested by the inflow-layer depths. Outside RMV, the inflow-layer

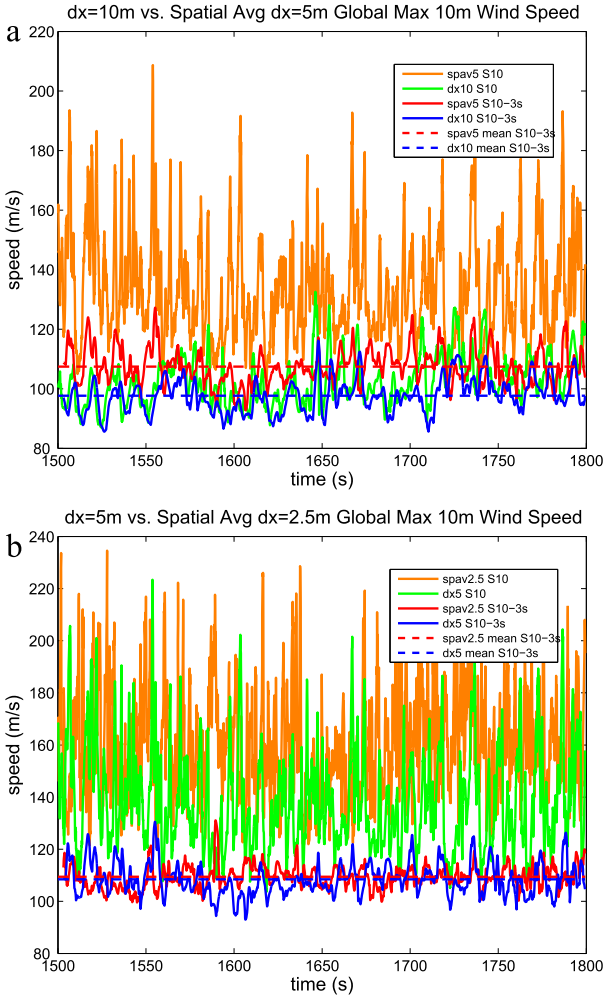

FIG. 4. Comparisons of peak instantaneous and 3-s horizontal wind gusts (S10 and S10-3s) for simulations of different resolutions, with the higher-resolution data first spatially averaged to the lower resolution: (a) CTRL10 vs spatially averaged CTRL; (b) CTRL vs spatially averaged CTRL2.5.

depth actually increases from CTRL20 (Fig. 3a) to CTRL10 (Fig. 3b) to CTRL (Fig. 1a) to CTRL2.5 (Fig. 3c), but the change from CTRL to CTRL2.5 is very small. The shapes of the magenta curves are quite similar for CTRL and CTRL2.5.

c. *Changes in vortex structure*

The size and structure of the vortex is strongly controlled by the rotation rate of the fluid in the far field, as determined by Ω, or equivalently S_r. Figure 5 shows the mean vortex and wind profiles for $S_r = 0.02$ (simulation SR02). Wind speeds $\{V\}_{\max}$ and $\{\mathrm{S10}\}_{\max}$ are reduced to 80.0 and 67.8 m s^{-1}, respectively, but RMS10 is nearly doubled, and values of $\{\mathrm{S10}\}$ greater than 60 m s^{-1} extend beyond $r = 500$ m. Consistent with many previous studies, this high-swirl vortex contains numerous asymmetries and smaller-scale vortices. One might suspect that the reduced mean intensity is simply a consequence of averaging over these asymmetries. However, the mean value of the peak surface gusts is also reduced from 108.5 (for CTRL) to 98.1 m s^{-1} (for SR02).

Snapshots of S10 and S10-3s are shown in Fig. 6. Not surprisingly, the S10 fields show a larger vortex with a greater number of localized wind maxima moving around the vortex. Time series of maximum S10 and S10-3s and W10 and W10-3s are also shown. Interestingly, Fig. 6d appears to show a larger disparity between the maximum values of W10 and W10-3s as compared to CTRL. W10 has large variability and frequently exceeds 100 m s^{-1}, while W10-3s has much less variability and stays near its mean value of 24 m s^{-1}. This suggests that, in comparison to CTRL, the fastest vertical winds are associated with smaller-scale features that are moving more quickly past fixed points at the surface. An example of such a feature will be shown in section 3d.

Figure 7 shows results for $S_r = 0.005$ (SR005). The vortex is both smaller and stronger, with RMV = 47.5 m and $\{V\}_{\max} = 104.9$ m s^{-1}. Comparison to the axisymmetric simulations of R16 indicate that this vortex is close to (but has slightly greater swirl than) the optimal swirl ratio that produces the most extreme values of $\{V\}_{\max}$ and $\{W\}_{\max}$ (see Fig. 6 of R16). An even more striking increase occurs for the mean peak gusts, which increase to 131.1 m s^{-1}. Fortunately, the area of the most destructive winds is drastically smaller for this vortex. In contrast to the larger vortices, which have RMS10 outside of RMV, in this case RMS10 is reduced to 27.5 m, well inside RMV (47.5 m), such that the area affected by the most destructive winds is less than 3% of the area for CTRL.

Fields of S10 and S10-3s also show the most destructive winds confined to a much smaller area for SR005 (Fig. 8). The structures of the S10 and S10-3s fields are more similar and the values are generally closer to each other. This is shown more clearly in the time series in Fig. 8c: maximum values of S10 and S10-3s are highly correlated and the 3-s gusts are not much less than the instantaneous values. This indicates that the peak winds, instantaneous or gusts, are actually representative of more stationary or lower-wavenumber asymmetries in the core, or even of the axisymmetric mean structure at the base of the vortex. W10 and W10-3s also show this similarity, with mean peak values of both in excess of 100 m s^{-1}.

d. *Extreme winds and suction vortices*

Given the extreme wind speeds produced by the model, we should consider whether these winds are produced by physically realistic flow structures and are

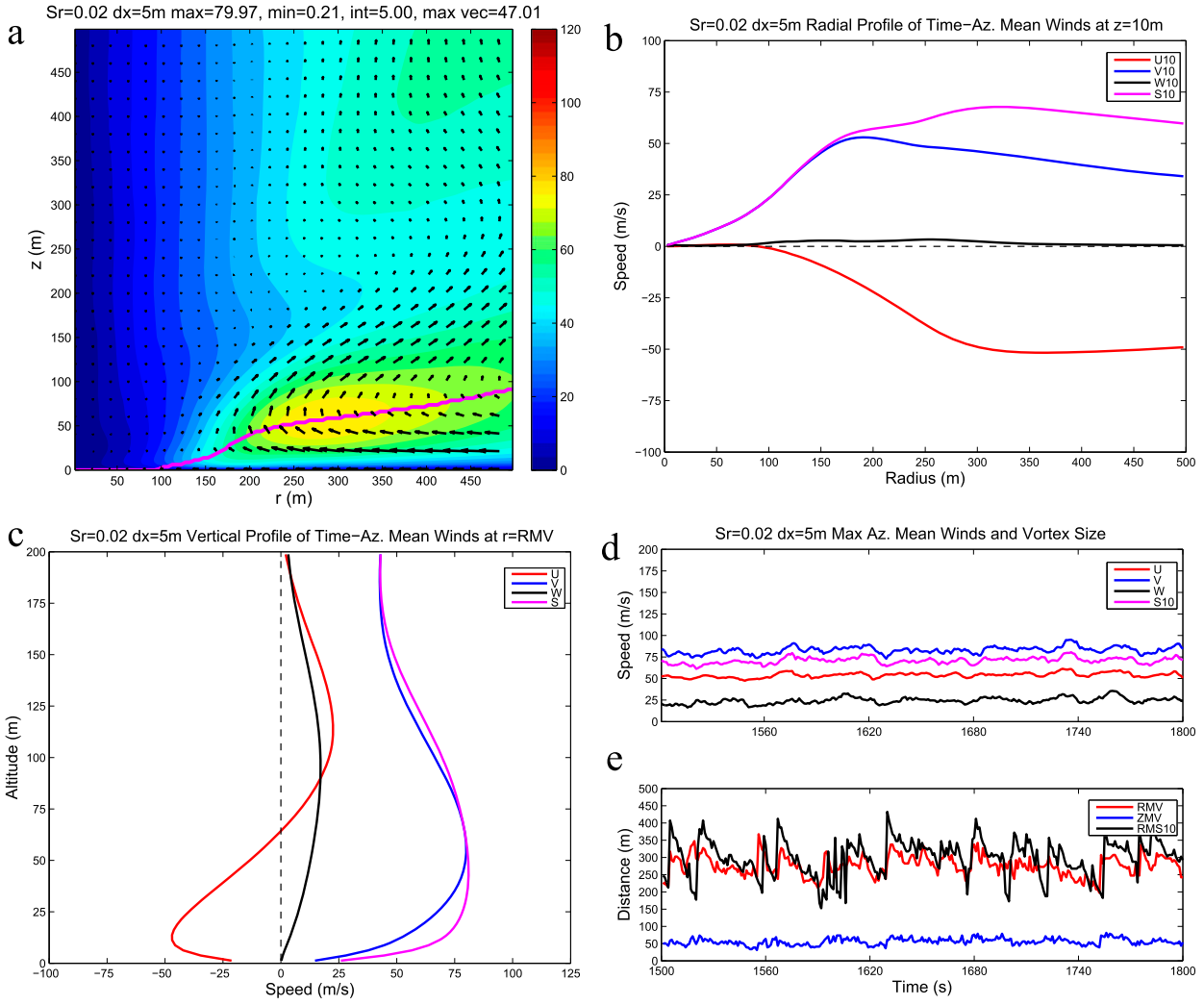

FIG. 5. As in Fig. 1, but for simulation SR02.

not associated with noise or other model artifacts. For most simulations, examination of the surface winds fields around the times of peak values of S10 and W10 reveals that the extreme winds are associated with smaller, transient vortices that rapidly form, intensify, and dissipate inside the RMV; these are widely known as suction vortices (Fujita 1970; Agee et al. 1977). As an illustration, we select the event of maximum S10 for CTRL, which occurs at $t = 1553.8$ s, as shown in Fig. 2c. Figure 9 shows a sequence of plots of instantaneous S10 (color) and W10 (white contours) in 0.5-s intervals leading up to this event. In the first snapshot (Fig. 9a), a preceding suction vortex is in the upper-right quadrant of the image, and in the next image, it reaches its peak intensity with S10 = 143 m s^{-1}. At the same time, a new vortex is beginning to form in the lower-left quadrant of the domain. In the next three intervals, the first vortex disappears completely, while the new vortex contracts and intensifies, reaching its peak intensity with S10 = 223 m s^{-1} and W10 = 165 m s^{-1}. In the last image, just 0.5 s later, this vortex appears to "break down" into a two-celled vortex, with downward motion at its center. A similar evolution was shown previously by Fiedler (1998).

Despite their great intensity, these vortices only contribute to a small fraction of the total kinetic energy (KE) of the wind field. For example, integrating the squared velocities of the two-dimensional wind field S10 over a 400 m × 400 m square centered on the CTRL vortex finds that the winds in excess of 150 m s^{-1} contribute to less than 1% of the total KE, while winds in excess of 100 m s^{-1} contribute about 15%.

Figure 10a shows a suction vortex from SR02. In this case, the mean vortex is much larger and the suction vortices are farther apart, so that only one suction vortex

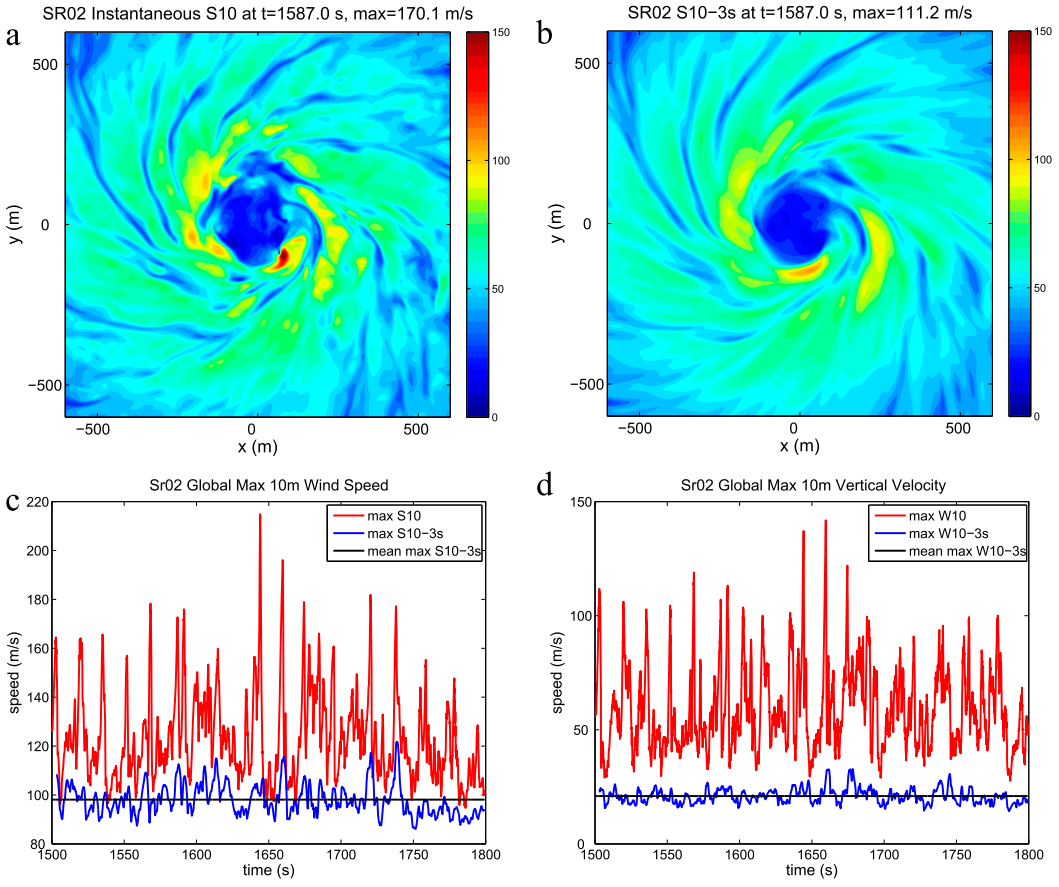

FIG. 6. As in Fig. 2, but for simulation SR02.

can appear in a plot domain with the same size as above. The broader spatial distribution of the vortices can be seen from the various local maxima in S10 shown in Fig. 6a. As the suction vortices in SR02 tend to be at larger radius, they move faster, and thus many of them are not actually closed circulations in terms of their ground-relative winds. Figure 10b shows a similar snapshot of S10 and W10 for SR005. Here, we do not see suction vortices, but rather the tornado itself is a single intense vortex that is only a little larger than the suction vortices of CTRL and SR02. The extreme gusts associated with this case, as shown in Fig. 8, are associated with rapid oscillations in the size and intensity of this vortex (see also Figs. 7d and 7e). Finally, Fig. 10c shows a snapshot from CTRL2.5, with suction vortices that are even smaller than in CTRL. While their instantaneous wind speeds are frequently greater than for CTRL, the 3-s gusts of S10 and W10 are not, as discussed above in section 3b.

e. *Changes in surface roughness*

Tornado structure and intensity are affected by the roughness of the underlying surface, which can range from grassy farmland to a fully urban environment. CTRL uses $z_0 = 0.2\,\text{m}$, and we now show results for $z_0 = 0.05$ and $0.8\,\text{m}$. Following standard guidance that roughness length can be associated with obstacles 10 times larger (e.g., Garratt 1992), we can see that such obstacles in CTRL would exceed the height of the first model level ($z = 1.25\,\text{m}$), and they would nearly reach $10\,\text{m}$ for $z_0 = 0.8\,\text{m}$. While the surface layer in this case would be better simulated with a modeling framework with embedded structures (e.g., Lewellen 2014), in the present modeling framework we can only change the surface roughness. Figure 11 shows time–azimuthal means as well as vertical profiles for $z_0 = 0.05$ and $0.8\,\text{m}$ (hereafter Z0-05 and Z0-8, respectively). For Z0-05, the boundary layer is shallower and $\{V\}_{\max}$ is closer to the surface; the opposite is true for Z0-8. This is also evident in the vertical profiles. Another interesting difference for Z0-8 is a significant reduction in the tangential winds near the surface and outside RMV, as also indicated by RMS10 in Table 2, which is about half the values for CTRL and Z0-05. Therefore, the mean wind fields suggest that this vortex would produce significantly

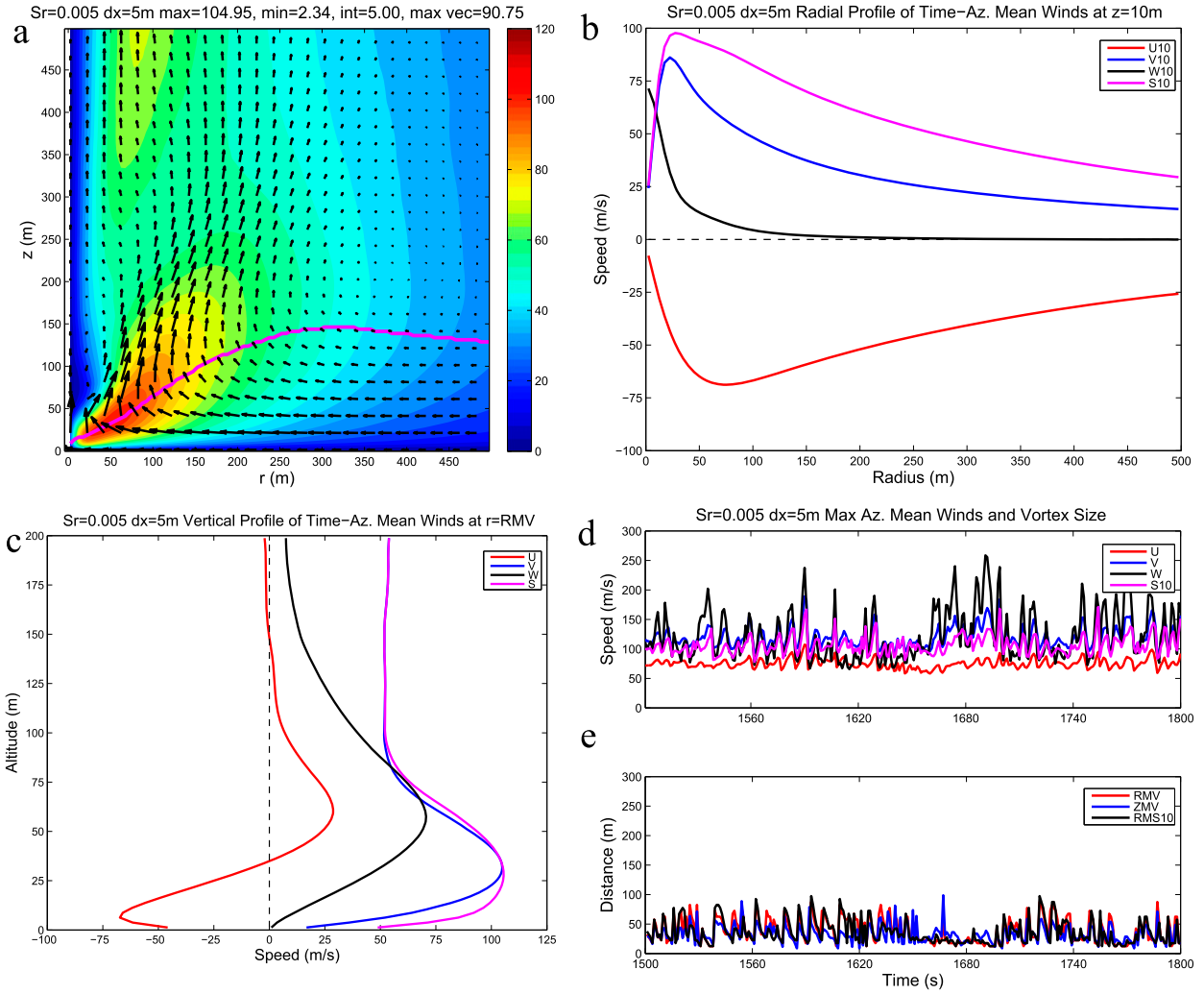

FIG. 7. As in Fig. 1, but for simulation SR005.

less damage than CTRL. Surprisingly, the mean peak gust is barely reduced (107.1 m s^{-1}) compared to CTRL (108.5 m s^{-1}) and Z0-05 (113.1 m s^{-1}), and the maximum gust is actually larger for Z0-08 (144.1 vs 133.8 m s^{-1}). Although slightly weaker and nearly half the size at the surface, the Z0-8 vortex appears to have about the same damage potential for individual structures as Z0-05 and CTRL. Such results may turn out differently in a model with resolved roughness elements or obstacles.

f. Changes in intensity

Theories for the mean intensity of a tornado-like vortex, such as those of Lilly (1969) and Fiedler and Rotunno (1986), suggest a linear scaling of intensity with increasing W_{conv} (which is proportional to the square root of the amplitude of the convective forcing). Approximately linear scaling was found in the axisymmetric, low–Reynolds number simulations of Nolan and Farrell (1999), with the ratio between $\{V\}_{\max}$ and W_{conv} approaching 1 from below for increasing W_{conv}. The higher-resolution, three-dimensional simulations of Fiedler (1998, 2009) also found this ratio to be close to 1, although those studies did not vary W_{conv} [the time–azimuthal-mean states of the Fiedler (2009) vortices are shown in Nolan (2012)].

Does this scaling hold for three-dimensional, fully turbulent vortices? According to the results shown in Fig. 12 and Table 2, it does. Simulations were performed with the convective forcing adjusted so that $W_{\text{conv}} = 40$, 60, and 100 m s^{-1} (W40, W60, and W100, respectively), but with Ω modified so that $S_r = \Omega l_r / W$ remains equal to 0.01. The shape of each vortex is remarkably similar among all four cases (W60 not shown), while the vortex size increases with Ω. The value of $\{V\}_{\max}$ is approximately 150% of W_{eff} for all four cases (see Tables 2 and 4). The mean surface winds $\{\text{Sl0}\}_{\max}$ show some

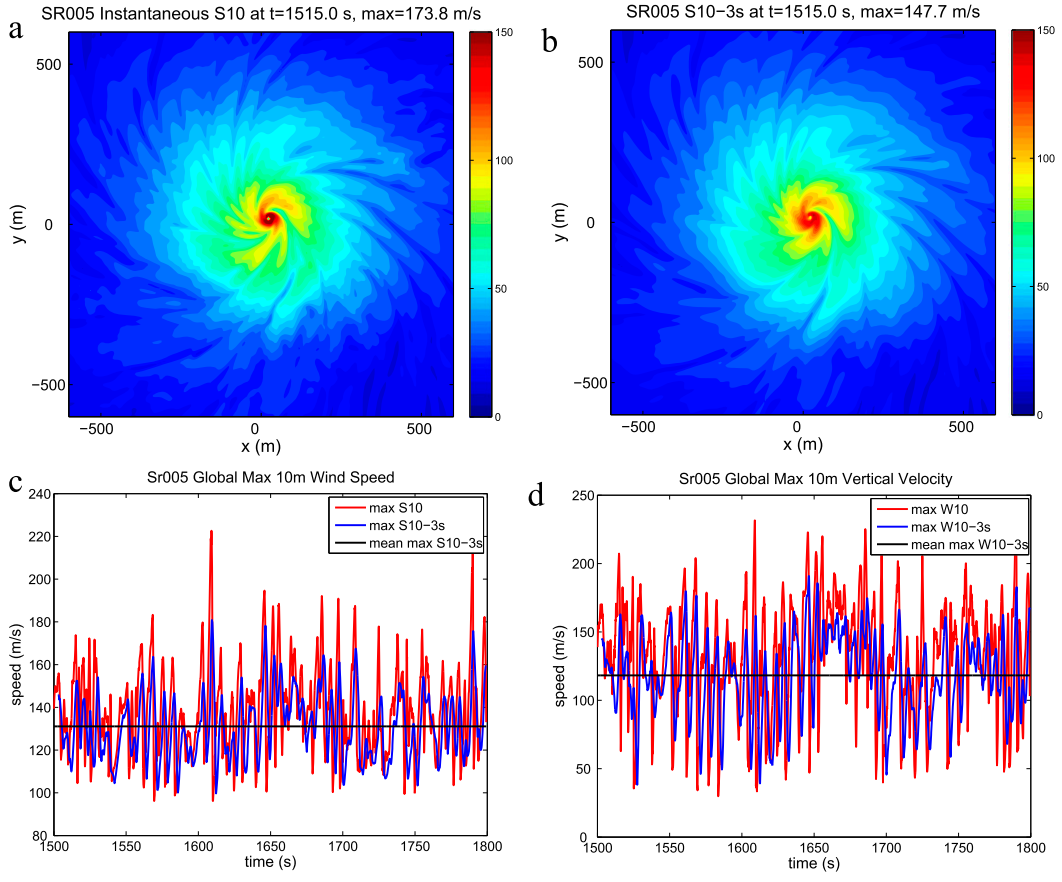

FIG. 8. As in Fig. 2, but for simulation SR005.

diminishing returns, being 139%, 126%, 121%, and 120% of their respective W_{eff} values. For the mean peak gusts, the relative values also diminish with intensity, being 192%, 179%, 165%, and 159% of W_{eff} (see also Table 3).

The increase in RMV with increasing W, despite adjusting Ω to maintain $S_r = 0.01$, is unexpected from simplistic scaling. Nolan (2005) argued that the circulation that is drawn into the vortex core varies like $\Gamma \sim \Omega l_r^2$, and therefore the expected RMV $\sim \Omega l_r^2/W$, and should not change if W and Ω vary together; this is equivalent to RMV $\sim S_r l_r$. This neglects the possible influence other nondimensional parameters listed in (7) of R16, particularly $\tau W/l_r$, which contains the damping layer relaxation time scale τ. To assess this, an additional W40 simulation was performed with τ adjusted so that $\tau W/Z_r$ was the same as for CTRL. This did produce a vortex of similar shape and intensity as W40 that was closer in size to CTRL (not shown).

g. *Comparisons to other simulations*

It is worthwhile to compare our results to the mean and transient velocities predicted by other LES studies of tornadoes. The most direct comparisons can be made to the results in the papers by Lewellen et al. (1997, 2000) and Lewellen and Lewellen (2007a,b). Since their simulations used smaller domains with fixed inflow and outflow boundary conditions, they could not compare to a convective forcing as measured by W_{conv} or W_{eff}. Rather, they used as their velocity scale the mean V in the ''upper core'' updraft region V_c, which is representative of the strength of the larger circulation above the corner flow region; the ratio $V_{\max}/V_c$ is a measure of the near-surface intensification caused by the tornado. This upper-core region appears in our simulations as the secondary maxima of $\{V\}$ that exist at and above $z = 500$ m at $r = 85$, 250, and 450 m for SR005, CTRL, SR02, respectively, and the values of V_c are 72, 63, and 57 m s^{-1} (in each case, these values are close to the mean $\{V\}$ farther aloft, from $z = 1000$ to 2000 m, not shown). Although these are similar to W_{conv} and W_{eff}, the fact that they vary with S_r means they are not precisely correlated with the convective forcing and that this scaling would make smaller, more intense vortices weaker in the nondimensional sense. Lewellen et al. (2000) do not state V_c for each case, although they do offer 75 m s^{-1} as a typical value. The

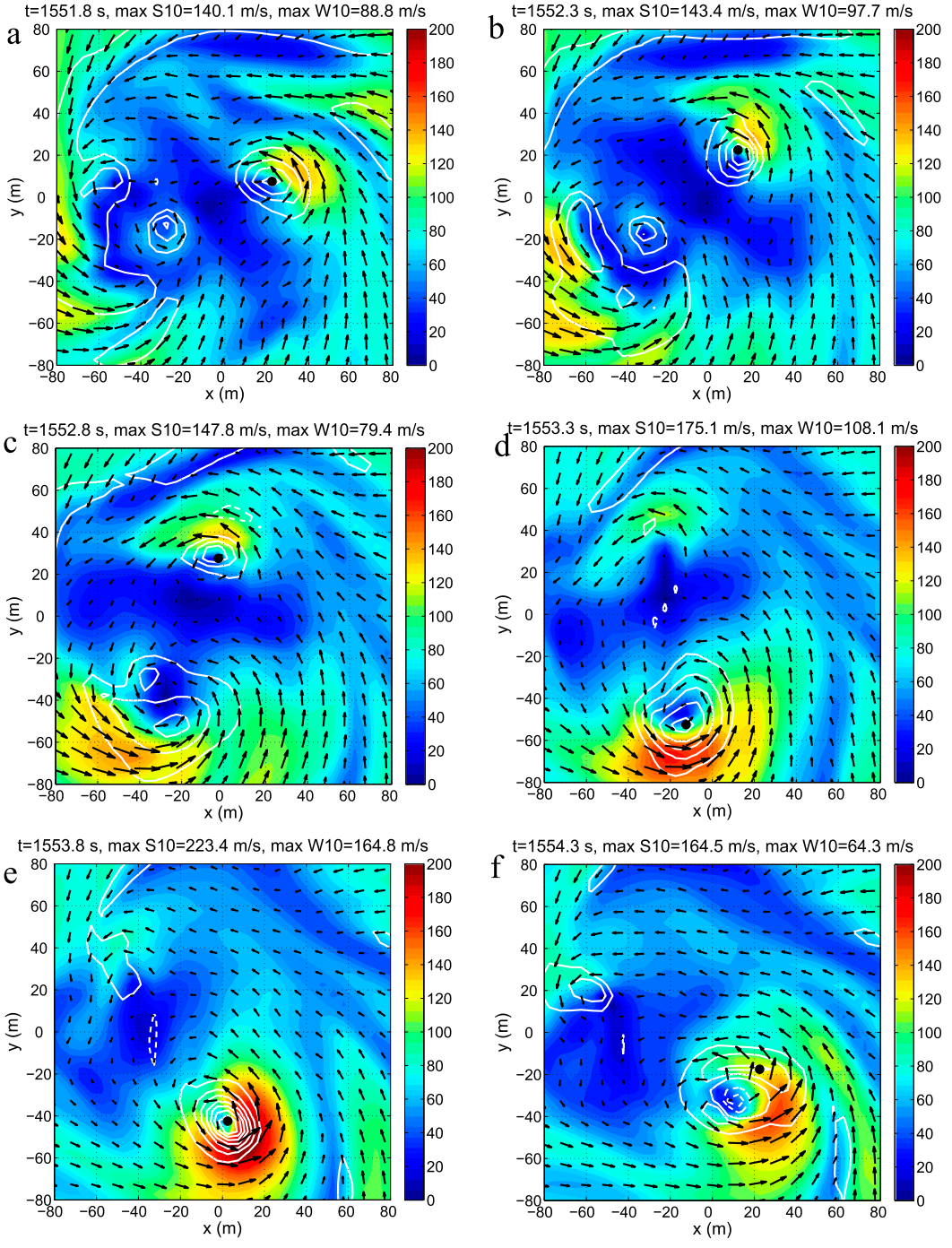

FIG. 9. Sequence every 0.5 s of S10 (colors) and W10 (white contours, 20 m s^{-1} intervals) leading to the most extreme value of S10 in CTRL, with times labeled above each plot. Each black dot indicates the location of maximum W10.

fastest V/V_c from that study is around 2.5, suggesting $\{V\}$ in excess of 200 m s^{-1}. This is substantially greater than our largest time-mean values of $\{V\}_{\max}$, even for W100.

In later studies of Lewellen and Lewellen (2007a,b), results were scaled by $V_s = \Gamma_\infty/r_d$, where Γ_∞ was the far-field circulation and r_d was the half-size of the computational domain, and it was stated that typical values of V_s ranged from 8 to 10 m s^{-1}. Those studies focused on transient intensification of vortices due to varying external conditions, with azimuthal-mean wind speeds $[V]_{\max}$ reaching $15V_s$. However, even in a quasi-steady

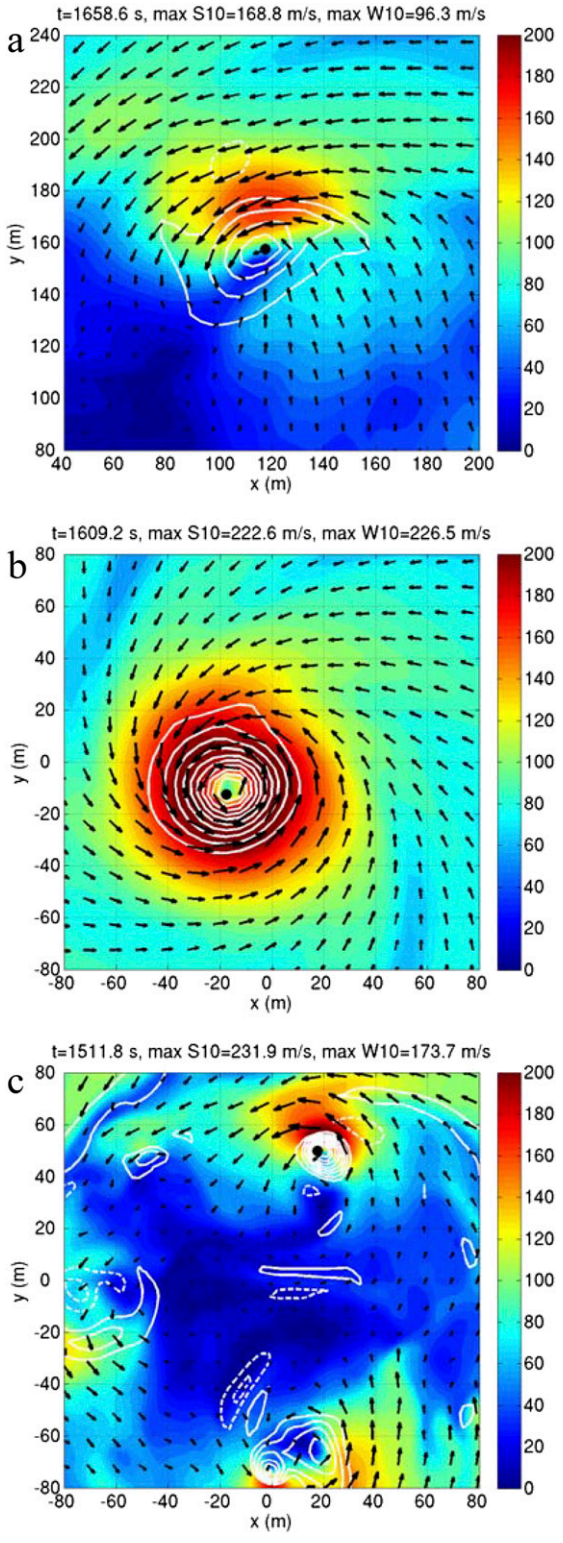

FIG. 10. As in Fig. 9, but for selected output times from other simulations: (a) SR02; (b) SR005; (c) CTRL2.5.

state, some transient axisymmetric oscillations in SR005 (see Fig. 7d) exceed 150 m s^{-1}, and thus the peak, transient, azimuthal-mean velocities in our simulations appear to reach nearly similar intensities. More recently, Lewellen et al. (2008) showed results of simulations with simulated debris loading. For their ''control'' case without debris $\{V\}_{\max} = 126\,\mathrm{m\,s^{-1}}$ compared to $V_c = 98\,\mathrm{m\,s^{-1}}$. That vortex is very small and intense, with RMV about 20 m and ZMV around 10 m.

Kuai et al. (2008) performed three-dimensional large-eddy simulations, modeled after a laboratory chamber using inflow and outflow boundary conditions but scaled up to the size of real tornadoes. Using inflow boundary conditions modeled after radar observations of the Spencer (1998) tornado analyzed by Wurman and Alexander (2005), they produced values of V at $z = 20$ m ($\{V20\}_{\max}$ in our notation) ranging from 45 to 176 m s^{-1}, depending on surface roughness and numerous other model parameters. Some of their simulations matched the size and intensity of the observed tornado (RMV = 120 m and $\{V20\}_{\max} = 81\,\mathrm{m\,s^{-1}}$) quite well. Again, direct comparison to these results is limited because of the very different model designs, but the mean low-level winds are quite similar.

Finally, Orf et al. (2017) produced a realistic, ''full physics'' supercell and tornado simulation with 30-m grid spacing over a very large domain, no surface friction, and an environmental CAPE which suggests $W_{\mathrm{conv}} = 99\,\mathrm{m\,s^{-1}}$ (which also equals W_{eff}, since there is no damping layer overlapping with the updraft zone). Instantaneous surface winds over 100 m s^{-1} are maintained for over 10 min, with a peak surface wind of 143 m s^{-1}. This ratio of maximum $S10$ to W_{eff}, about 1.4, is less than what occurs in most of our simulations, which ranges from 1.8 to 2.8.

4. Momentum budgets and the effects of resolved turbulence

The results indicate that a steady-state tornado-like vortex can support mean intensities—both aloft and at the surface—well above the so-called thermodynamic speed limit represented by W_{eff} (the maximum possible updraft speed). This occurs despite the effects of three-dimensional asymmetries that are continuously developing from the strong instability of the mean state (Nolan 2012), some of which break down into smaller eddies and turbulence. As shown in B17, most of the turbulent mixing is associated with eddies that are well resolved in these simulations. What role do the eddies play in the mean intensity? Are eddies only working to

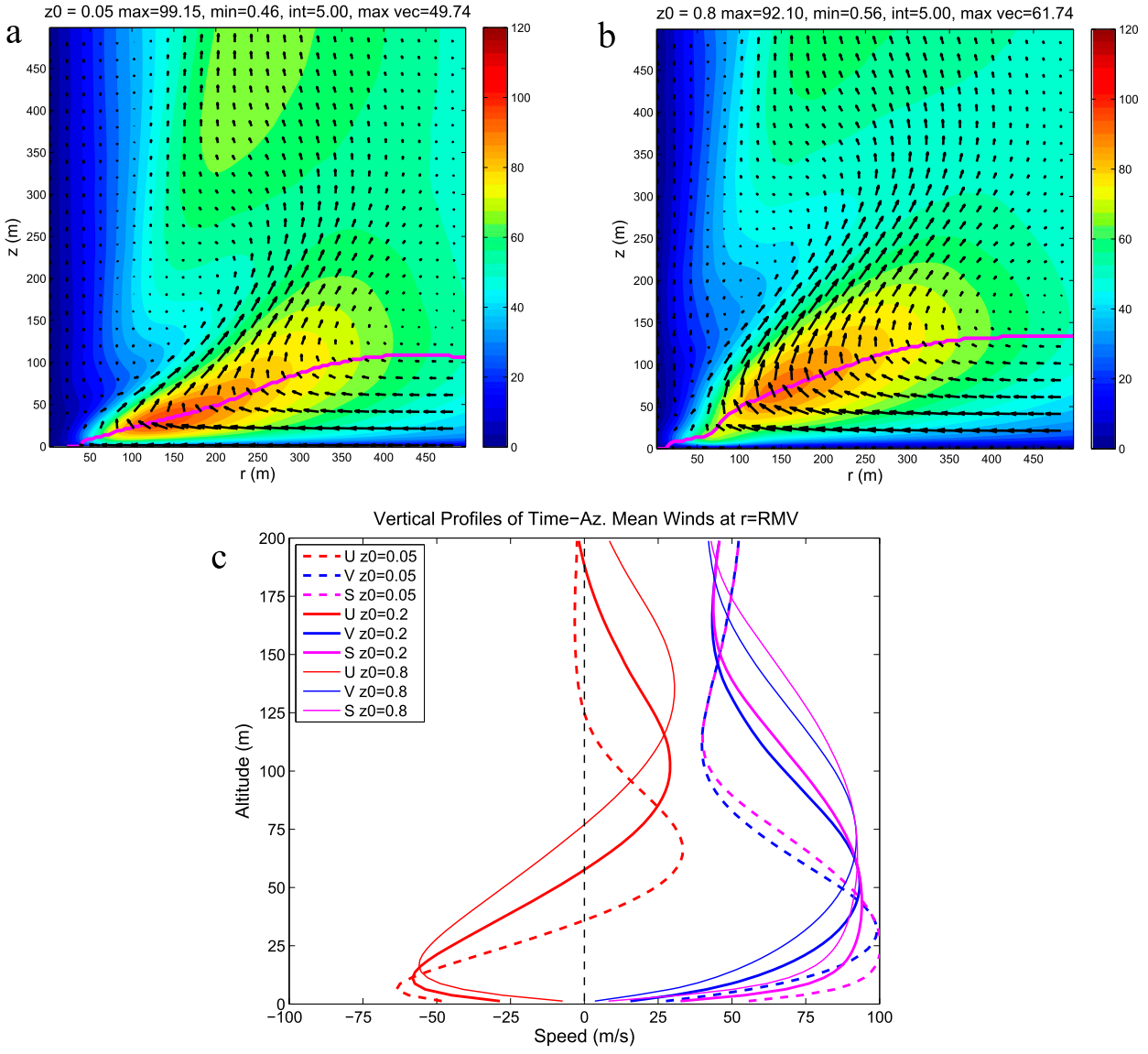

FIG. 11. Time–azimuthal-mean wind fields for simulations with different roughness lengths: (a) Z0-05 ($z_0 = 0.05$ m); (b) Z0-8 ($z_0 = 0.8$ m); (c) vertical profiles of winds at r = RMV, including CTRL with $z_0 = 0.2$ m.

diminish it? Or are they somehow intensifying the peak winds, perhaps through upgradient momentum transports?

To investigate the roles of eddies and turbulence in the vortex core, we compute each of the terms that appear in equations for the time-averaged azimuthal-mean flows:

$$\frac{\Delta[U]}{\tau} = -\{U\}\frac{\partial\{U\}}{\partial r} - \{W\}\frac{\partial\{U\}}{\partial r} + \frac{\{V^2\}}{r} - \frac{\partial\{\phi\}}{\partial r} - \frac{1}{r}\frac{\partial}{\partial r}\{rU'^2\} - \frac{\partial}{\partial z}\{U'W'\} + \frac{\{V'^2\}}{r} + 2\Omega\{V\} + \{F_u\}, \quad (4.1)$$

$$\frac{\Delta[V]}{\tau} = -\{U\}\frac{\partial\{V\}}{\partial r} - \{W\}\frac{\partial\{V\}}{\partial z} - \frac{\{UV\}}{r} - \frac{1}{r^2}\frac{\partial}{\partial r}\{r^2U'V'\} - \frac{\partial}{\partial z}\{V'W'\} - 2\Omega\{U\} + \{F_v\}, \quad \text{and} \quad (4.2)$$

$$\frac{\Delta[W]}{\tau} = -\{U\}\frac{\partial\{W\}}{\partial r} - \{W\}\frac{\partial\{W\}}{\partial z} - \frac{\partial\{\phi\}}{\partial z} - \frac{1}{r}\frac{\partial}{\partial r}\{rU'W'\} - \frac{\partial}{\partial z}\{W'^2\} + \{F_w\}, \quad (4.3)$$

where, as above, the rectangular brackets refer to azimuthal means and the curly brackets refer to azimuthal

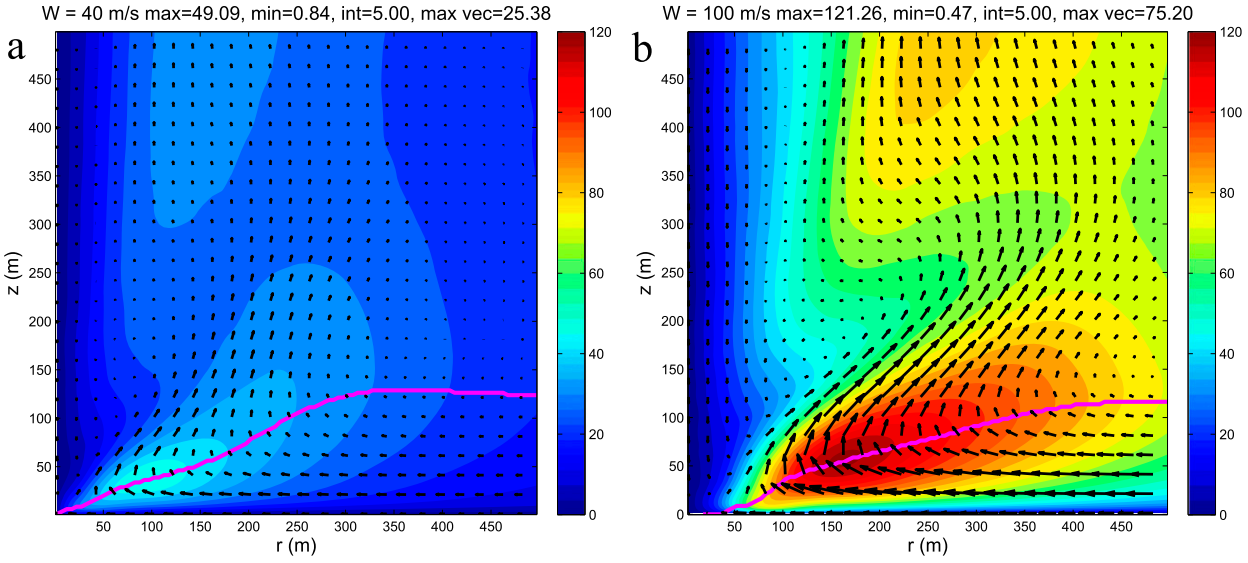

FIG. 12. Time–azimuthal-mean wind fields for simulations with different convective forcing: (a) W40 and (b) W100.

and temporal means. As shown in (1d) of R16, ϕ is the density-normalized pressure. The F terms refer to the tendencies due to the subgrid-scale turbulence scheme. Each term on the left-hand side is the net change in the azimuthal-mean wind field over the averaging period τ (equal to 5 min for our calculations). Ideally, for steady-state tornadoes, these would be small and converge to zero for large τ.

For this analysis we used the same averaging procedure used by B17, which makes the calculations less sensitive to the definition of the vortex center. First, the three-dimensional flow was time averaged over 300 s of model output every 1 s. Deviations from this time-mean state were computed on the Cartesian grid. Then, time-mean flows and products of their perturbations were transformed into cylindrical coordinates about the center point of the domain (directly below the center of the convective forcing). Finally, all fields were azimuthally averaged.

Special treatment is required for the subgrid-scale turbulence terms. These are computed in CM1 from parameterized eddy stresses in Cartesian coordinates; for example, $\tau_{xy} = \overline{u_s v_s}$, where here u_s, v_s, and w_s are unresolved subgrid-scale velocity fluctuations in the x, y, and z directions, and the overbar represents a grid-scale spatial average. To properly convert the stress terms, the variables u_s, v_s, and w_s must be related to subgrid-scale velocities in cylindrical coordinates, U_s, V_s, and W_s, as follows:

$$U_s = \frac{u_s x + v_s y}{r}, \quad V_s = \frac{v_s x - u_s y}{r}, \quad \text{and} \quad W_s = w_s. \tag{4.4}$$

Substitution of these expressions into the six eddy flux terms gives the parameterized eddy stresses in terms of the Cartesian subgrid-scale stresses computed by CM1:

$$\begin{aligned} \overline{U_s^2} &= \overline{u_s^2}\left(\frac{x}{r}\right)^2 + 2\overline{u_s v_s}\left(\frac{xy}{r^2}\right) + \overline{v_s^2}\left(\frac{y}{r}\right)^2 \\ &= \frac{1}{r^2}(\tau_{xx}x^2 + 2\tau_{xy}xy + \tau_{yy}y^2), \end{aligned} \tag{4.5}$$

TABLE 4. Relative axisymmetric mean or gust intensities. Ratios of maximum velocities to either the effective convective velocity scale W_{eff} or to the time–azimuthal-mean tangential velocity $\{V\}_{\max}$. An asterisk indicates the same value as for the control simulation (CTRL).

Name	W_{eff} (m s^{-1})	Effective CAPE (J kg^{-1})	$\{V\}_{\max}/W_{\text{eff}}$	$\{\text{S10}\}_{\max}/\{V\}_{\max}$	Mean max S10-3s/$\{V\}_{\max}$	Max S10-3s/$\{V\}_{\max}$
CTRL	65.8	2164	1.42	0.85	1.16	1.40
SR02	*	*	1.21	0.85	1.22	1.52
SR005	*	*	1.59	0.93	1.25	1.72
Z0-8	*	*	1.40	0.76	1.16	1.56
Z0-05	*	*	1.50	0.93	1.14	1.35
W40	31.3	489	1.56	0.88	1.22	1.55
W60	48.5	1176	1.48	0.85	1.21	1.46
W100	84.0	3528	1.44	0.83	1.10	1.29

$$\overline{V_s^2} = \overline{v_s^2}\left(\frac{x}{r}\right)^2 - 2\overline{u_s v_s}\left(\frac{xy}{r^2}\right) + \overline{u_s^2}\left(\frac{y}{r}\right)^2$$
$$= \frac{1}{r^2}(\tau_{yy}x^2 - 2\tau_{xy}xy + \tau_{xx}y^2), \quad (4.6)$$

$$\overline{W_s^2} = \overline{w_s^2} = \tau_{zz}, \quad (4.7)$$

$$\overline{U_s V_s} = \overline{u_s v_s}\left[\left(\frac{x}{r}\right)^2 - \left(\frac{y}{r}\right)^2\right] + (\overline{v_s^2} - \overline{u_s^2})\frac{xy}{r^2}$$
$$= \frac{1}{r^2}[\tau_{xy}(x^2 - y^2) + (\tau_{yy} - \tau_{xx})xy], \quad (4.8)$$

$$\overline{U_s W_s} = \overline{u_s w_s}\frac{x}{r} + \overline{v_s w_s}\frac{y}{r} = \frac{1}{r}(\tau_{xz}x + \tau_{yz}y), \quad \text{and} \quad (4.9)$$

$$\overline{V_s W_s} = \overline{v_s w_s}\frac{x}{r} + \overline{u_s w_s}\frac{y}{r} = \frac{1}{r}(\tau_{yz}x + \tau_{xz}y). \quad (4.10)$$

The subgrid-scale tendencies $\{F_u\}$, $\{F_v\}$, and $\{F_w\}$ in (4.1)–(4.3) are computed from the same divergence operations to these terms that are applied to the resolved eddies in those equations.

We first consider U and V momentum budgets for CTRL shown in Fig. 13. The six panels show (i) the mean advective terms; (ii) the sum of pressure, Coriolis, and Centripetal forces; (iii) tendencies due to radial eddy fluxes; (iv) tendencies due to vertical eddy fluxes; (v) tendencies due to subgrid-scale turbulence; and (vi) the residual. Ideally, the last term would be zero everywhere.

Looking first at the V budget, the advective and rotational terms are exactly as expected, making large and approximately compensating tendencies that are opposite in sign on either side of the axis of maximum V. The subgrid tendency is negative but is significant only in a very shallow layer near the surface. This strongly supports our claim (as in B17) that the large majority of turbulent mixing is accomplished by resolved eddies (except very near the surface). Of greatest interest are the radial and vertical eddy tendencies. Both of these are negative along the axis of maximum V, showing that eddies are indeed working to weaken $\{V\}_{\max}$. They also show positive tendencies inside and above the axis of maximum V, indicating that eddies are predominantly transporting angular momentum inward and upward. A similar result for eddy fluxes and their tendencies on V was shown by Lewellen et al. (1997). The tendencies on W from radial and vertical fluxes (not shown) also show that eddies are transporting positive vertical momentum into the relatively stagnant core of the vortex.

To maintain $\{V\}_{\max}$ against turbulent diffusion, U must be negative there; therefore, the effect of eddy mixing on U at this location is also relevant. The third panel of the U budget shows that the U tendency due to radial eddy fluxes is positive, or outward, so again it is clear that eddies are working to weaken V in the vortex core. Another interesting aspect of the U budget is that the layer of net negative imbalance between the pressure force and the centripetal force is remarkably shallow, less than 20 m deep, even though the radial inflow extends up to the location of $\{V\}_{\max}$. If this figure is extended out to larger radius (not shown), then the layer of net inward force becomes much deeper, driving the inward acceleration of radial inflow. Near the RMV, however, the centripetal force is far larger than the pressure force (except in the thin surface layer) and the inflow is maintained by strong inward radial advection of the negative radial momentum that parcels in the middle and upper boundary layer have accumulated as they accelerate into the vortex.

Returning to the V budget, the vertical eddy fluxes generate a layer of positive tendency near the surface that extends outward to beyond $r = 250$ m. This shows that eddies in the boundary layer are transporting angular momentum downward and are ''spinning up'' the tangential flow near the surface. The same result can be seen in Fig. 15 of B17, which shows increasing downward transport of momentum by resolved eddies as the boundary layer flow moves toward the vortex center.

How much does the eddy-injection lead to enhanced mixing by resolved eddies? To answer this, the total (radial and vertical) eddy tendency and the subgrid tendency on V are shown in Fig. 14 for CTRL and for an identical simulation that did not use eddy injection. Two differences are apparent. First, the near-surface positive tendency extends to much larger radius for CTRL than for the no-eddy-injection case. Second, the maximum negative eddy tendency inside the RMV is larger (-16 vs $-10\,\mathrm{m\,s^{-2}}$) for CTRL, again suggesting that there is more redistribution of momentum by resolved eddies when eddy injection is used.

The V budgets for SR02 and SR005 are shown in Fig. 15. The SR02 budget is very similar to CTRL, but with tendencies of weaker amplitude extending to larger radii. As for CTRL, downward transport of angular momentum into the lower boundary layer is evident.

Computing budgets for SR005 was problematic. The much smaller and more intense vortex does not remain near the domain center but, rather, executes half of a cyclonic loop during the period when data were recorded, with displacements from the domain center ranging from 10 to 100 m. Several variations on the method of computing the momentum budgets were evaluated, such as the method described above (time averaging first), or one based on tracking the vortex center, computing azimuthal means and perturbations about that center, and then taking time averages. This latter method produced what we would subjectively call the best results: it leaves

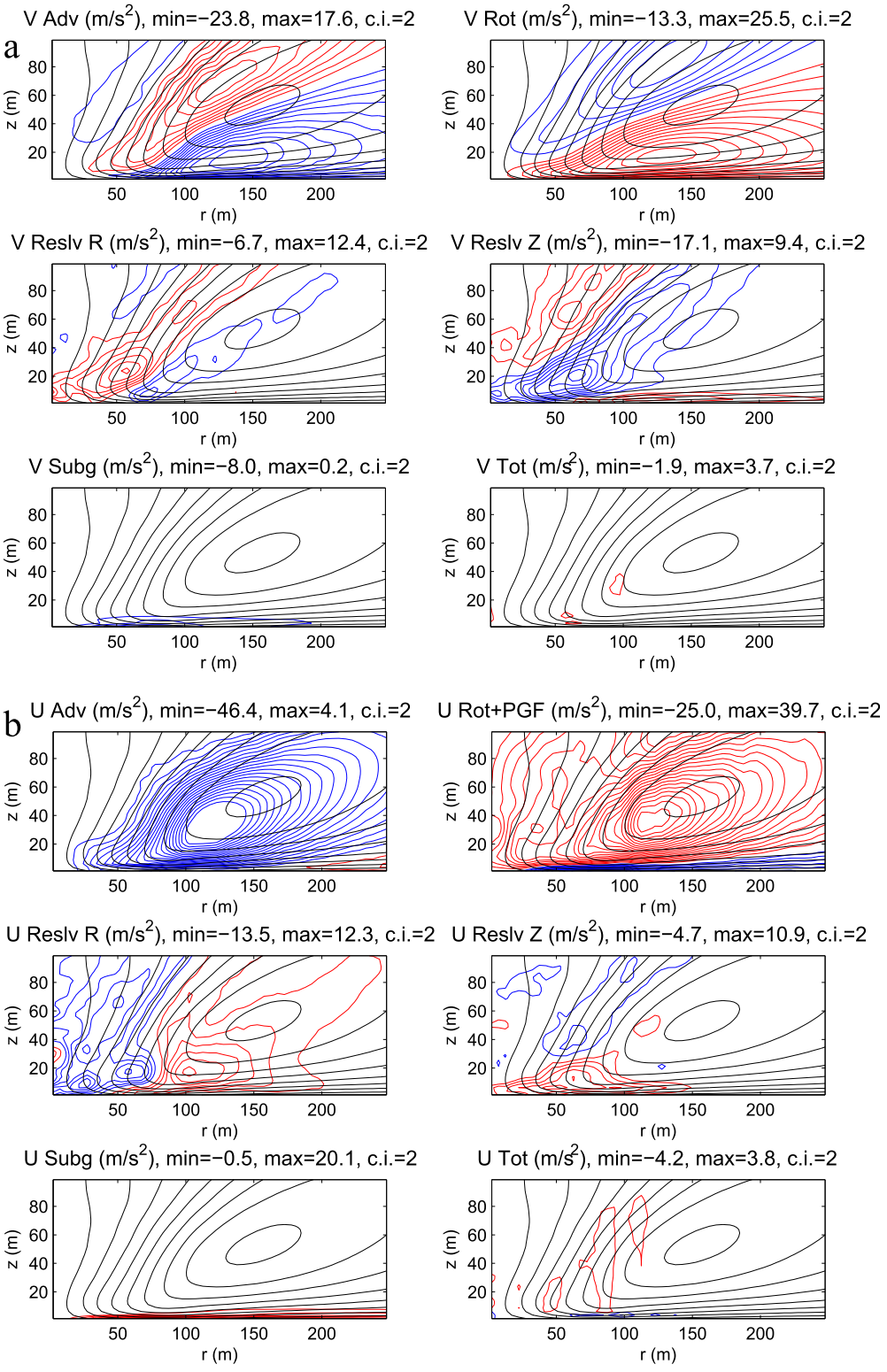

FIG. 13. Time–azimuthal-mean tendencies on (a) tangential velocity V and (b) radial velocity U due to azimuthal-mean terms, resolved eddies separated into radial and vertical fluxes, parameterized eddies, and the total (or residual) tendency, for simulation CTRL. Red contours indicate positive values and blue contours indicate negative values, both with 2 m s^{-2} intervals. The black contours show the time- and azimuthal-mean tangential winds with contour intervals of 10 m s^{-1}.

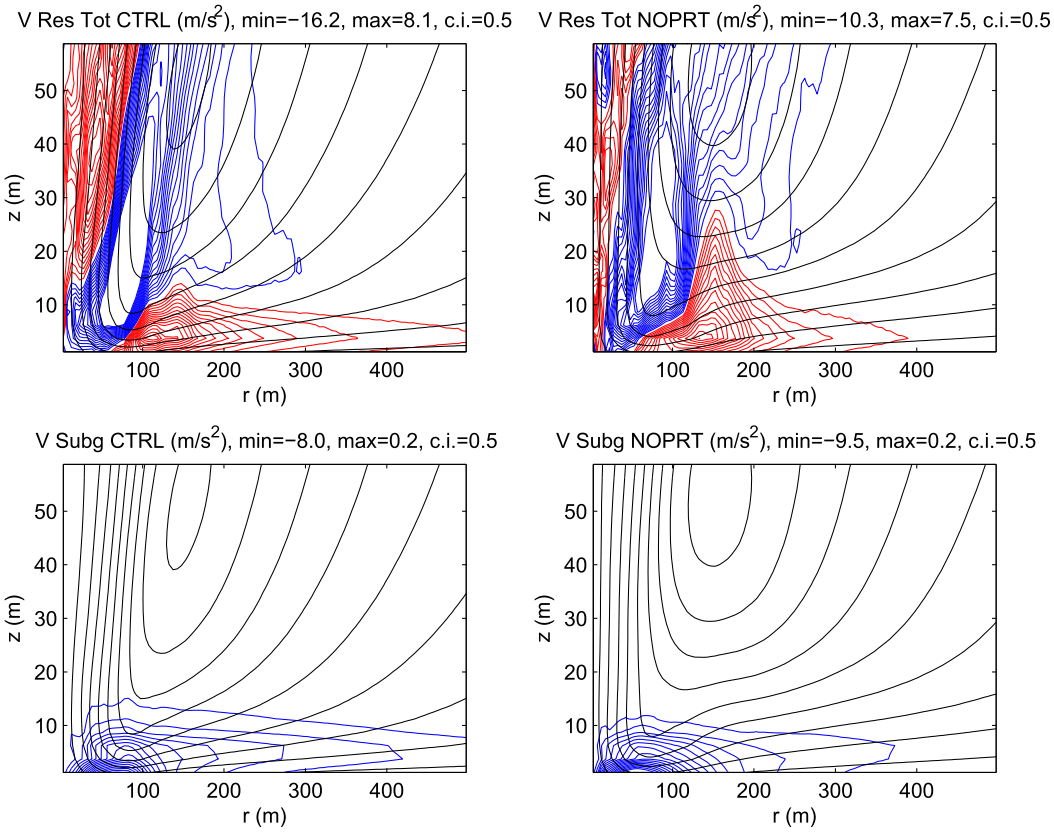

FIG. 14. Time–azimuthal-mean tendencies on V by (top) resolved and (bottom) parameterized eddies, for (left) CTRL and (right) a similar simulation without eddy injection. Contours are as in Fig. 13, but with a contour interval of 0.5 m s^{-2}.

very large residuals, but these are confined to within 20 m of the vortex center. This result is shown for the V budget in Fig. 15b. Ignoring the large residuals near $r = 0$, the same conclusions as above can be drawn: eddies redistribute angular momentum inward and upward from the axis of maximum $\{V\}$, they also transport angular momentum into the lower boundary layer, and their tendencies dominate over subgrid-scale mixing except in the lowest 10 m.

5. Mean winds, surface winds, and damage areas

Suppose that during a field experiment, a tornado is well observed by one or more Doppler radars and an accurate analysis can be made of the azimuthal-mean V field down to at least the upper part of the inflow layer, either using dual-Doppler or GBVTD techniques. The tornado occurs over uninhabited terrain, with no significant structures to damage. If the maximum azimuthal-mean wind $\{V\}_{\max}$ is analyzed to be 90 m s^{-1} at a radius of RMV = 150 m (i.e., similar to CTRL), what kinds of mean and transient winds probably happened at the surface?

The answer still depends on many unknowns, but our results provide some guidance. The maximum azimuthal-mean total wind speed at the surface $\{\text{S10}\}_{\max}$ would be less, ranging from 70 m s^{-1} over a rougher landscape to as much as 84 m s^{-1} over smooth terrain. The maximum transient, 3-s horizontal wind gusts at any one time at the surface would typically be around 105 m s^{-1}, but could occasionally reach as high as 125 m s^{-1}. Peak vertical wind gusts at 10 m would average 30 m s^{-1} but could reach as high as 60 m s^{-1}.

These are very extreme wind speeds. In retrospect, the azimuthal-mean intensities of the CTRL, SR02, and SR005 cases may be representative of only the strongest tornadoes. The strongest azimuthal-mean winds analyzed to date by GBVTD analyses are 70–85 m s^{-1} (Lee and Wurman 2005; Kosiba et al. 2008; Kosiba and Wurman 2010), generally less than the values of 80–105 m s^{-1} in our simulations. The W60 simulation is probably more typical, with $\{V\}_{\max}$ = 72 m s^{-1}, $\{\text{S10}\}_{\max}$ = 61.3 m s^{-1}, mean maximum S10-3s = 86.9 m s^{-1}, and maximum S10-3s = 105.1 m s^{-1}.

Some of these relationships are summarized in Table 4. The third column compares $\{V\}_{\max}$ to W_{eff}, which can in

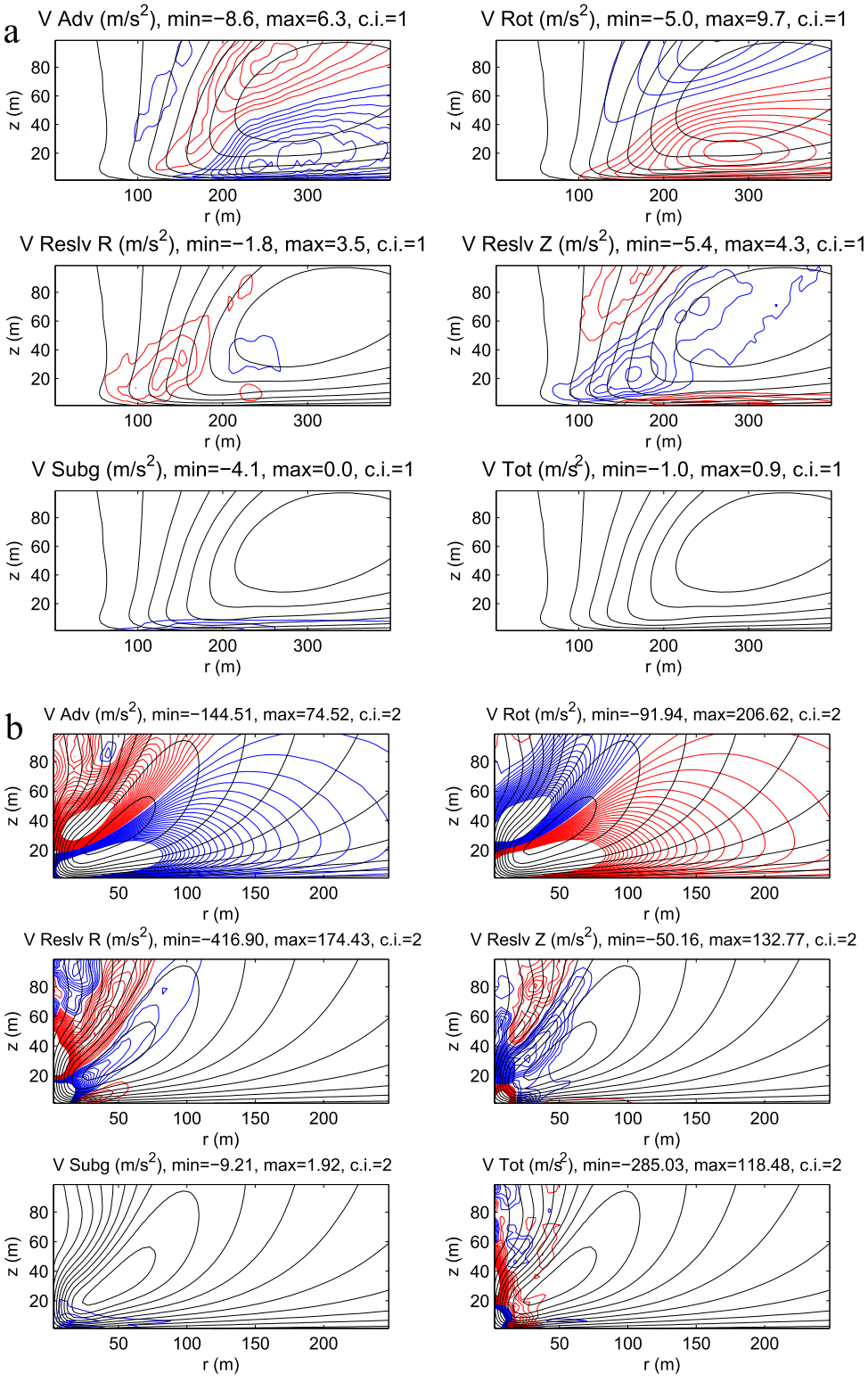

FIG. 15. Time–azimuthal-mean tendencies on V due to azimuthal-mean terms, resolved eddies separated into radial and vertical fluxes, parameterized eddies, and the total (or residual) tendency, for simulations (a) SR02 and (b) SR005.

turn be related to environmental convective instability through CAPE = $W_{\text{eff}}^2/2$. The remaining columns compare the other intensities to $\{V\}_{\max}$. We choose this comparison rather than to W_{eff} since in our thought experiment $\{V\}_{\max}$ is the most reliably observed quantity. Perhaps what stands out most from Table 4 is the relatively small variations among the wind speed ratios across the various cases. For example, mean S10-3s/$\{V\}_{\max}$ varies only from 1.10 to 1.22. The value of $\{V\}_{\max}/W_{\text{eff}}$ varies mostly from 1.42 to 1.59. The one exception is the high-swirl tornado of SR02 with a ratio of 1.21. In contrast, the low-swirl tornado of SR005 is by far the most intense vortex in every way.

For the larger vortices of CTRL and SR02, comparisons of the radial profiles of S10 (Figs. 1b and 5b) to the snapshots of S10-3s (Figs. 2b and 6b) indicate that the strongest wind gusts occur well inside the radius of maximum mean surface wind. For example, while RMS10 = 177.5 m in CTRL, Fig. 2b shows that gusts in excess of 100 m s^{-1} typically occur inside of r = 100 m. This is clearly not the case for the smaller, low-swirl configuration of SR005, where the typical locations of the maximum azimuthal-mean S10, maximum S10-3s, and instantaneous values of S10 are all close to each other, inside of r = 50 m (Figs. 7b, 7d, and 8b).

The thought experiment can be taken in the other direction: suppose there are no direct wind observations of a tornado, but surveys reveal several locations of EF4-level damage, indicating frequent 3-s gusts in the range of 74–90 m s^{-1} (WSEC 2006). If the tornado were a medium swirl vortex with an RMV of about 150 m, then we can estimate $\{V\}_{\max}$ using the ratio shown in Table 4; that is, $\{V\}_{\max}$ = 82 m s^{-1}/1.16 = 71 m s^{-1} (where 82 m s^{-1} is the middle value of the EF4 range). If the vortex was larger, it would have required greater $\{V\}_{\max}$ to generate similar damage; but if near the optimal state, it could have been considerably weaker.

6. Summary and conclusions

In this study we have revisited the relationships between convective forcing, tornado structure, and tornado intensity using a new modeling framework and more relevant measures of tornado intensity. The new modeling framework consists of the Fiedler chamber approach of using a large domain and a fixed vertical forcing function, along with the injection of realistic turbulent perturbations into the boundary layer to ensure that turbulence is fully developed in the tornado boundary layer. Above a very thin surface layer the large majority of the redistribution of momentum in the boundary layer is associated with model-resolved eddies [see Bryan et al. (2017) for a full discussion].

The time- and azimuthal-mean tangential wind $\{V\}_{\max}$ in these simulated tornadoes range from 20% to 60% greater than the velocity scale W_{eff} associated with the effective convective forcing. Velocity scale W_{eff} is defined as the maximum velocity of parcels freely traveling up the central axis of the convective forcing in simulations without rotation and is diminished from the analytically expected value W_{conv} by an upper-level damping layer (see appendix A of R16). Values of W_{eff} ranging from 31 to 84 m s^{-1} produce vales of $\{V\}_{\max}$ ranging from 49 to 121 m s^{-1}. The largest ratio of $\{V\}_{\max}$ to W_{eff}, 1.59, occurs for the "low swirl" vortex of simulation SR005, which is also significantly smaller in size (see Table 2). These mean wind speeds are similar to those published in previous LES studies, such as Lewellen et al. (2000) and Lewellen and Lewellen (2007a,b), accounting for the different modeling frameworks and scalings, and they are also similar to—though generally larger than—peak axisymmetric winds produced from GBVTD analyses of tornadoes observed with portable Doppler radars (Lee and Wurman 2005; Kosiba et al. 2008; Kosiba and Wurman 2010).

To assess the role of resolved and parameterized eddies in the tornado cores and their effects on intensity, comprehensive budgets of angular, radial, and vertical momentum in tornado cores were computed. Not surprisingly, the peak tangential winds are produced by the large inward transport and radially inward overshoot of angular momentum in the upper boundary layer, which is driven by the imbalance between inward pressure forces and diminished centrifugal forces in the lower boundary layer. Resolved eddies transport both positive angular momentum and negative radial momentum inward and upward, reducing $\{V\}_{\max}$, spinning up the flow near the center axis and bringing faster tangential winds closer to the surface.

While the peak tangential winds at the top of the boundary layer have been occasionally observed by portable Doppler radars, we use these simulations to estimate the mean and transient surface winds (defined at z = 10 m) that might actually be occurring for a given value of $\{V\}_{\max}$ and other parameters. For each case, three measures of intensity were computed that are representative of the low-level wind and the damage it might cause: the time–azimuthal-mean horizontal surface wind speed $\{\text{S10}\}_{\max}$; the time mean of the maximum horizontal wind gusts S10-3s occurring anywhere; and the time mean of the maximum vertical wind gusts W10-3s. The value of $\{\text{S10}\}_{\max}$ is generally about 15% less than $\{V\}_{\max}$ but increases with decreasing surface roughness. Values of maximum S10-3s are, on average, 10%–20% greater than $\{V\}_{\max}$, but S10-3s can occasionally be 40%–50% greater than $\{V\}_{\max}$. The

simulations show surprisingly large values for vertical velocities only 10 m above the surface: typically the maximum values of W10-3s are about 33% of $\{V\}_{\max}$—for example, 20–30 m s^{-1}, with transient values exceeding 50 m s^{-1}.

Just as $\{V\}_{\max}/W_{\text{eff}}$ was larger for SR005, the mean and transient gusts are also significantly greater compared to $\{V\}_{\max}$. Mean and maximum values of peak S10-3s are 25% and 72% greater than the already enhanced $\{V\}_{\max}$. Thankfully, however, these extreme winds are confined to much smaller areas than for the larger, higher-swirl vortices.

The tornadoes simulated in this study are highly idealized. They suffer no potential limiting effects from unsteady convective forcing, an unsteady or asymmetric supply of rotating air, spatially varying surface roughness, significant surface features such as trees or buildings, nor significant debris loading. Two recent studies simulated tornadoes with embedded debris, using different methods: Lewellen et al. (2008) treated the air and debris mixture as a ''two fluid'' system, whereas Bodine et al. (2016) represented debris with large numbers of Lagrangian particles. Both studies found that the debris field reduced $\{V\}_{\max}$ by as much as 50% for heavy loadings (where ''heavy'' means that the mass of debris becomes comparable to the mass of air per unit volume). These results suggest our simulations overestimate the intensity of actual quasi-steady tornadoes—either in terms of azimuthal-mean winds or 3-s gusts—as compared to W_{eff} and its equivalent CAPE. Of course, a slower but debris-heavy wind field might well do more damage than an unloaded but faster wind field.

For the purposes of understanding or even predicting damages caused by tornadoes, the surface winds and surface gusts are more important than the azimuthal-mean winds aloft; however, it is only the latter that can be measured with any reliability. To our knowledge, this study is the first to systematically evaluate relationships between $\{V\}_{\max}$ and horizontal and vertical wind gusts at the surface, using the important step of converting all wind speeds to 3-s gusts sustained at fixed points. Maximum values of peak surface winds over a period of time can be highly infrequent, so we argue that it is the time mean of the peak wind that is most representative of damage potential. An extreme 3-s gust that occurs where there are no structures does no additional damage, is virtually unobservable, and may not be representative of the vast majority of gusts. This logic really only applies to the case of a moving tornado, where the core area of high surface winds and gusts remain over a given area or structure for a short period of time. In a subsequent paper, we simulate tornadoes moving across the surface (Dahl et al. 2017). From these simulations we estimate the likelihood that a fixed structure will experience various levels of wind intensity and how these probabilities change with tornado intensity, size, and structure.

Acknowledgments. The authors thank D. Lewellen and two anonymous reviewers for their comments that led to significant improvements of this manuscript. This work was supported in part by the National Science Foundation through Grant AGS-1265899. We acknowledge high-performance computing support from Yellowstone (ark:/85065/d7wd3xhc) provided by the Computational and Information Systems Laboratory of the National Center for Atmospheric Research.

REFERENCES

Agee, E. M., J. T. Snow, F. S. Nickerson, P. R. Clare, C. R. Church, and L. A. Schaal, 1977: An observational study of the West Lafayatte, Indiana, tornado of 20 March 1976. *Mon. Wea. Rev.*, **105**, 893–907, doi:10.1175/1520-0493(1975)103<0318:SSAADF>2.0.CO;2.

Alexander, C. R., and J. M. Wurman, 2008: Updated mobile radar climatology of supercell tornado structures and dynamics. *24th Conf. on Severe Local Storms*, Savannah, GA, Amer. Meteor. Soc., 19.4. [Available online at https://ams.confex.com/ams/24SLS/techprogram/paper_141821.htm.]

Atkins, N. T., K. M. Butler, K. R. Flynn, and R. M. Wakimoto, 2014: An integrated damage, visual, and radar analysis of the 2013 Moore, Oklahoma, EF5 tornado. *Bull. Amer. Meteor. Soc.*, **95**, 1549–1561, doi:10.1175/BAMS-D-14-00033.1.

Blair, S. F., D. R. Deroche, and A. E. Pietrycha, 2008: In situ observations of the 21 April 2007, Tulia, Texas tornado. *Electron. J. Severe Storms Meteor.*, **3** (3). [Available online at http://www.ejssm.org/ojs/index.php/ejssm/article/view/39.]

Blanchard, D. O., 2013: A comparison of wind speed and forest damage associated with tornadoes in northern Arizona. *Wea. Forecasting*, **28**, 408–417, doi:10.1175/WAF-D-12-00046.1.

Bluestein, H. B., and J. H. Golden, 1993: A review of tornado observations. *The Tornado: Its Structure, Dynamics, Prediction, and Hazards*, *Geophys. Monogr.*, Vol. 79, Amer. Geophys. Union, 319–352, doi:10.1029/GM079p0319.

——, W. P. Unruh, J. LaDue, H. Stein, and D. Speheger, 1993: Doppler radar wind spectra of supercell tornadoes. *Mon. Wea. Rev.*, **121**, 2200–2222, doi:10.1175/1520-0493(1993)121<2200:DRWSOS>2.0.CO;2.

——, W.-C. Lee, M. Bell, C. C. Weiss, and A. L. Pazmany, 2003: Mobile Doppler radar observations of a tornado in a supercell near Bassett, Nebraska, on 5 June 1999. Part II: Tornado-vortex structure. *Mon. Wea. Rev.*, **131**, 2968–2984, doi:10.1175/1520-0493(2003)131<2968:MDROOA>2.0.CO;2.

Bodine, D. J., T. Maruyama, R. D. Palmer, C. J. Fulton, and H. B. Bluestein, 2016: Sensitivity of tornado dynamics to soil debris loading. *J. Atmos. Sci.*, **73**, 2783–2801, doi:10.1175/JAS-D-15-0188.1.

Brasseur, J. G., and T. Wei, 2010: Designing large-eddy simulation of the turbulent boundary layer to capture law-of-the-wall scaling. *Phys. Fluids*, **22**, 021303, doi:10.1063/1.3319073.

Bryan, G. H., and J. M. Fritsch, 2002: A benchmark simulation for moist nonhydrostatic numerical models. *Mon. Wea. Rev.*, **130**, 2917–2928, doi:10.1175/1520-0493(2002)130<2917:ABSFMN>2.0.CO;2.

——, N. A. Dahl, D. S. Nolan, and R. Rotunno, 2017: An eddy injection method for large-eddy simulations of tornado-like vortices. *Mon. Wea. Rev.*, **145**, 1937–1961, doi:10.1175/MWR-D-16-0339.1.

Burgess, D., and Coauthors, 2014: 20 May 2013 Moore, Oklahoma, tornado: Damage survey and analysis. *Wea. Forecasting*, **29**, 1229–1237, doi:10.1175/WAF-D-14-00039.1.

Dahl, N. A., D. S. Nolan, G. H. Bryan, and R. Rotunno, 2017: Using high-resolution simulations to quantify underestimates of tornado intensity from in situ observations. *Mon. Wea. Rev.*, **145**, 1963–1982, doi:10.1175/MWR-D-16-0346.1.

Davies-Jones, R., R. J. Trapp, and H. B. Bluestein, 2001: Tornadoes and tornadic storms. *Severe Convective Storms*, *Meteor. Monogr.*, No. 50, Amer. Meteor. Soc., 167–221.

Dowell, D. C., C. R. Alexander, J. M. Wurman, and L. J. Wicker, 2005: Centrifuging of hydrometeors and debris in tornadoes: Radar-reflectivity patters and wind-measurement errors. *Mon. Wea. Rev.*, **133**, 1501–1524, doi:10.1175/MWR2934.1.

Fiedler, B. H., 1994: The thermodynamic speed limit and its violation in axisymmetric numerical simulations of tornado-like vortices. *Atmos.–Ocean*, **32**, 335–359, doi:10.1080/07055900.1994.9649501.

——, 1998: Wind-speed limits in numerical simulated tornadoes with suction vortices. *Quart. J. Roy. Meteor. Soc.*, **124**, 2377–2392, doi:10.1002/qj.49712455110.

——, 2009: Suction vortices and spiral breakdown in numerical simulations of tornado-like vortices. *Atmos. Sci. Lett.*, **10**, 109–114, doi:10.1002/asl.217.

——, and R. Rotunno, 1986: A theory for the maximum windspeeds in tornado-like vortices. *J. Atmos. Sci.*, **43**, 2328–2340, doi:10.1175/1520-0469(1986)043<2328:ATOTMW>2.0.CO;2.

Fujita, T. T., 1970: The Lubbock tornadoes: A study of suction spots. *Weatherwise*, **23**, 161–173, doi:10.1080/00431672.1970.9932888.

Garratt, J. R., 1992: *The Atmospheric Boundary Layer.* Cambridge University Press, 316 pp.

Howells, P. A. C., R. Rotunno, and R. K. Smith, 1988: A comparative study of atmospheric and laboratory-analogue numerical tornado-vortex models. *Quart. J. Roy. Meteor. Soc.*, **114**, 801–822, doi:10.1002/qj.49711448113.

Karstens, C. D., W. A. Gallus, B. D. Lee, and C. A. Finley, 2013: Analysis of tornado-induced tree-fall using aerial photography from the Joplin, Missouri, and Tuscaloosa-Birmingham, Alabama, tornadoes of 2011. *J. Appl. Meteor. Climatol.*, **52**, 1049–1068, doi:10.1175/JAMC-D-12-0206.1.

Kepert, J. D., 2001: The dynamics of boundary-layer jets within the tropical cyclone core. Part I: Linear theory. *J. Atmos. Sci.*, **58**, 2469–2484, doi:10.1175/1520-0469(2001)058<2469:TDOBLJ>2.0.CO;2.

Kosiba, K., and J. Wurman, 2010: Three-dimensional axisymmetric wind field structure of the Spencer, South Dakota, 1998 tornado. *J. Atmos. Sci.*, **67**, 3074–3083, doi:10.1175/2010JAS3416.1.

——, and ——, 2013: The three-dimensional structure and evolution of a tornado boundary layer. *Wea. Forecasting*, **28**, 1552–1561, doi:10.1175/WAF-D-13-00070.1.

——, R. J. Trapp, and J. Wurman, 2008: An analysis of the axisymmetric three-dimensional low level wind field in a tornado using mobile radar observations. *Geophys. Res. Lett.*, **35**, L05805, doi:10.1029/2007GL031851.

Kuai, L., F. L. Haan, W. A. Gallus Jr., and P. P. Sarkar, 2008: CFD simulations of the flow field of a laboratory-simulated tornado for parameter sensitivity studies and comparison with field measurements. *Wind Struct.*, **11**, 75–96, doi:10.12989/was.2008.11.2.075.

Landsea, C. W., and J. L. Franklin, 2013: Atlantic hurricane database uncertainty and presentation of a new database format. *Mon. Wea. Rev.*, **141**, 3576–3592, doi:10.1175/MWR-D-12-00254.1.

Lee, W.-C., and J. Wurman, 2005: Diagnosed three-dimensional axisymmetric structure of the Mulhall tornado on 3 May 1999. *J. Atmos. Sci.*, **62**, 2373–2393, doi:10.1175/JAS3489.1.

——, B. J.-D. Jou, P.-L. Chang, and S.-M. Deng, 1999: Tropical cyclone kinematic structure retrieved from single-Doppler radar observations. Part I: Interpretation of Doppler velocity patterns and the GBVTD technique. *Mon. Wea. Rev.*, **127**, 2419–2439, doi:10.1175/1520-0493(1999)127<2419:TCKSRF>2.0.CO;2.

Lewellen, D. C., 2014: Local roughness effects on tornado dynamics. *27th Conf. on Severe Local Storms*, Madison, WI, Amer. Meteor. Soc., 15A.1. [Available online at https://ams.confex.com/ams/27SLS/webprogram/Paper254357.html.]

——, and W. S. Lewellen, 2007a: Near-surface intensification of tornado vortices. *J. Atmos. Sci.*, **64**, 2176–2194, doi:10.1175/JAS3965.1.

——, and ——, 2007b: Near-surface intensification through corner flow collapse. *J. Atmos. Sci.*, **64**, 2195–2209, doi:10.1175/JAS3966.1.

——, ——, and J. Xia, 2000: The influence of a local swirl ratio on tornado intensification near the surface. *J. Atmos. Sci.*, **57**, 527–544, doi:10.1175/1520-0469(2000)057<0527:TIOALS>2.0.CO;2.

——, B. Gong, and W. S. Lewellen, 2008: Effects of finescale debris on near-surface tornado dynamics. *J. Atmos. Sci.*, **65**, 3247–3262, doi:10.1175/2008JAS2686.1.

Lewellen, W. S., D. C. Lewellen, and R. I. Sykes, 1997: Large-eddy simulation of a tornado's interaction with the surface. *J. Atmos. Sci.*, **54**, 581–605, doi:10.1175/1520-0469(1997)054<0581:LESOAT>2.0.CO;2.

Lilly, D. K., 1969: Tornado dynamics. NCAR Manuscript 69-117, 39 pp. [Available online at https://opensky.ucar.edu/islandora/object/manuscripts%3A870/datastream/PDF/view.]

Nolan, D. S., 2005: A new scaling for tornado-like vortices. *J. Atmos. Sci.*, **62**, 2639–2645, doi:10.1175/JAS3461.1.

——, 2012: Three-dimensional instabilities in tornado-like vortices with secondary circulations. *J. Fluid Mech.*, **711**, 61–100, doi:10.1017/jfm.2012.369.

——, 2013: On the use of Doppler radar–derived wind fields to diagnose the secondary circulations of tornadoes. *J. Atmos. Sci.*, **70**, 1160–1171, doi:10.1175/JAS-D-12-0200.1.

——, and B. F. Farrell, 1999: The structure and dynamics of tornado-like vortices. *J. Atmos. Sci.*, **56**, 2908–2936, doi:10.1175/1520-0469(1999)056<2908:TSADOT>2.0.CO;2.

——, J. A. Zhang, and E. W. Uhlhorn, 2014: On the limits of estimating maximum wind speeds in hurricanes. *Mon. Wea. Rev.*, **142**, 2814–2837, doi:10.1175/MWR-D-13-00337.1.

Orf, L., R. Wilhelmson, B. Lee, C. Finley, and A. Houston, 2017: Evolution of a long-track violent tornado within a simulated supercell. *Bull. Amer. Meteor. Soc.*, **98**, 45–68, doi:10.1175/BAMS-D-15-00073.1.

Rasmussen, E. N., J. M. Straka, R. P. Davies-Jones, C. A. Doswell, F. H. Carr, M. D. Eilts, and D. R. MacGorman, 1994: Verification of the Origins of Rotation in Tornadoes Experiment: VORTEX. *Bull. Amer. Meteor. Soc.*, **75**, 995–1006, doi:10.1175/1520-0477(1994)075<0995:VOTOOR>2.0.CO;2.

Rotunno, R., 1979: A study in tornado-like vortex dynamics. *J. Atmos. Sci.*, **36**, 140–155, doi:10.1175/1520-0469(1979)036<0140:ASITLV>2.0.CO;2.

——, 2013: The fluid dynamics of tornadoes. *Annu. Rev. Fluid Mech.*, **45**, 59–84, doi:10.1146/annurev-fluid-011212-140639.

——, G. H. Bryan, D. S. Nolan, and N. A. Dahl, 2016: Axisymmetric tornado simulations at high Reynolds number. *J. Atmos. Sci.*, **73**, 3843–3853, doi:10.1175/JAS-D-16-0038.1.

Snyder, J. C., and H. B. Bluestein, 2014: Some considerations for the use of high-resolution mobile radar data in tornado intensity determination. *Wea. Forecasting*, **29**, 799–827, doi:10.1175/WAF-D-14-00026.1.

Sullivan, P. P., J. C. McWilliams, and C.-H. Moeng, 1994: A subgrid-scale model for large eddy simulations of planetary boundary-layer flows. *Bound.-Layer Meteor.*, **71**, 247–276, doi:10.1007/BF00713741.

Tanamachi, R. L., H. B. Bluestein, W.-C. Lee, M. Bell, and A. Pazmany, 2007: Ground-based velocity-track display (GBVTD) analysis of W-band Doppler radar data in a tornado near Stockton, Kansas, on 15 May 1999. *Mon. Wea. Rev.*, **135**, 783–800, doi:10.1175/MWR3325.1.

Wakimoto, R. M., P. Stauffer, W.-C. Lee, N. T. Atkins, and J. Wurman, 2012: Finescale structure of the LaGrange, Wyoming, tornado during VORTEX2: GBVTD and photogrammetric analysis. *Mon. Wea. Rev.*, **140**, 3397–3418, doi:10.1175/MWR-D-12-00036.1.

Weiss, C. C., T. Cermak, R. Metzger, A. Reinhart, and P. Skinner, 2014: Insights into tornado structure afforded by high-frequency mobile radar. *27th Conf. on Severe Local Storms*, Madison, WI, Amer. Meteor. Soc., 9.4. [Available online at https://ams.confex.com/ams/27SLS/webprogram/Paper255350.html.]

WSEC, 2006: A recommendation for an enhanced Fujita scale (EF-scale). Texas Tech University Wind Science and Engineering Center Rep., 108 pp. [Available online at http://www.depts.ttu.edu/nwi/Pubs/Fscale/EFScale.pdf.]

Wurman, J., 1998: Some preliminary results from the ROTATE-98 tornado experiment. Preprints, *19th Conf. on Severe Local Storms*, Minneapolis, MN, Amer. Meteor. Soc., 120–123.

——, 2008: Preliminary results and report of the ROTATE-2008 radar/in-situ/mobile mesonet experiment. *24th Conf. on Severe Local Storms*, Savannah, GA, Amer. Meteor. Soc., 5.4. [Available online at https://ams.confex.com/ams/24SLS/techprogram/paper_142200.htm.]

——, and C. R. Alexander, 2005: The 30 May Spencer, South Dakota, storm. Part II: Comparison of observed damage and radar-derived winds in the tornadoes. *Mon. Wea. Rev.*, **133**, 97–119, doi:10.1175/MWR-2856.1.

——, J. M. Straka, and E. N. Rasmussen, 1996: Fine-scale Doppler radar observations of tornadoes. *Science*, **272**, 1774–1777, doi:10.1126/science.272.5269.1774.

——, C. Alexandre, P. Robinson, and Y. Richardson, 2007: Low-level winds in tornadoes and potential catastrophic tornado impacts in urban areas. *Bull. Amer. Meteor. Soc.*, **88**, 31–46, doi:10.1175/BAMS-88-1-31.

——, D. Dowell, Y. Richardson, P. Markowski, E. Rasmussen, D. Burgess, L. Wicker, and H. B. Bluestein, 2012: The second Verification of the Origins of Rotation in Tornadoes Experiment: VORTEX2. *Bull. Amer. Meteor. Soc.*, **93**, 1147–1170, doi:10.1175/BAMS-D-11-00010.1.

——, K. Kosiba, and P. Robinson, 2013: In situ, Doppler radar, and video observations of the interior structure of a tornado and the wind–damage relationship. *Bull. Amer. Meteor. Soc.*, **94**, 835–846, doi:10.1175/BAMS-D-12-00114.1.

Xia, J., W. S. Lewellen, and D. C. Lewellen, 2003: Influence of Mach number on tornado corner flow dynamics. *J. Atmos. Sci.*, **60**, 2820–2825, doi:10.1175/1520-0469(2003)060<2820:IOMNOT>2.0.CO;2.

Zhang, J. A., R. F. Rogers, D. S. Nolan, and F. D. Marks, 2011: On the characteristic height scales of the hurricane boundary layer. *Mon. Wea. Rev.*, **139**, 2523–2535, doi:10.1175/MWR-D-10-05017.1.